

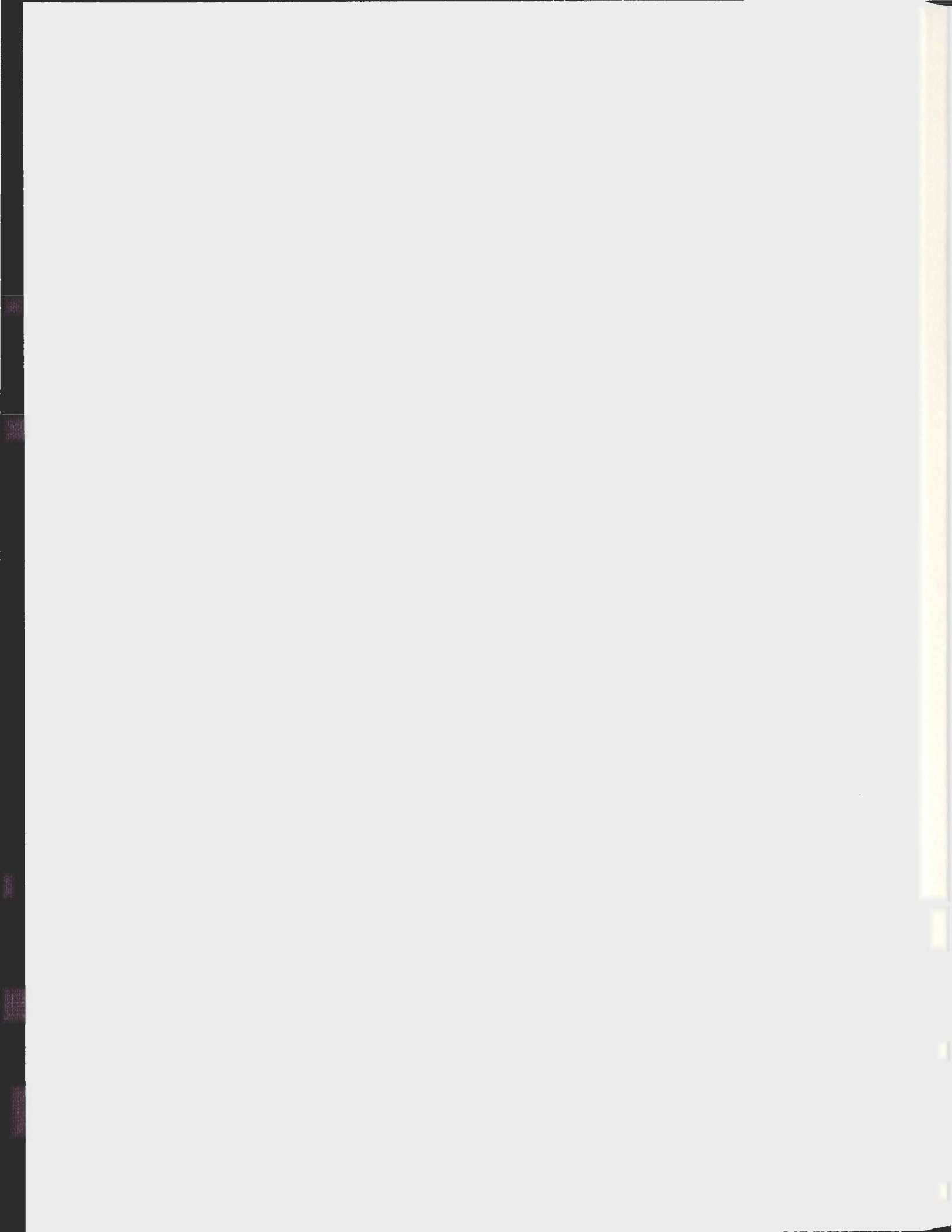
QUANTUM CHEMISTRY AND RAMAN SPECTROSCOPY
STUDIES OF ANION HYDRATION

CENTRE FOR NEWFOUNDLAND STUDIES

**TOTAL OF 10 PAGES ONLY
MAY BE XEROXED**

(Without Author's Permission)

J.D.C. CRAIG





National Library
of Canada

Bibliothèque nationale
du Canada

Acquisitions and
Bibliographic Services

Acquisitions et
services bibliographiques

395 Wellington Street
Ottawa ON K1A 0N4
Canada

395, rue Wellington
Ottawa ON K1A 0N4
Canada

Your file *Votre référence*

ISBN: 0-612-89618-8

Our file *Notre référence*

ISBN: 0-612-89618-8

The author has granted a non-exclusive licence allowing the National Library of Canada to reproduce, loan, distribute or sell copies of this thesis in microform, paper or electronic formats.

L'auteur a accordé une licence non exclusive permettant à la Bibliothèque nationale du Canada de reproduire, prêter, distribuer ou vendre des copies de cette thèse sous la forme de microfiche/film, de reproduction sur papier ou sur format électronique.

The author retains ownership of the copyright in this thesis. Neither the thesis nor substantial extracts from it may be printed or otherwise reproduced without the author's permission.

L'auteur conserve la propriété du droit d'auteur qui protège cette thèse. Ni la thèse ni des extraits substantiels de celle-ci ne doivent être imprimés ou autrement reproduits sans son autorisation.

In compliance with the Canadian Privacy Act some supporting forms may have been removed from this dissertation.

Conformément à la loi canadienne sur la protection de la vie privée, quelques formulaires secondaires ont été enlevés de ce manuscrit.

While these forms may be included in the document page count, their removal does not represent any loss of content from the dissertation.

Bien que ces formulaires aient inclus dans la pagination, il n'y aura aucun contenu manquant.

Canada

Quantum Chemistry and Raman Spectroscopy Studies of Anion Hydration

© J. D. C. Craig

A thesis submitted to the School of Graduate Studies
in partial fulfilment of the requirements for
the degree of Master of Science

Department of Chemistry
Faculty of Science
Memorial University of Newfoundland

April MM

St. John's

Newfoundland

Abstract

The low frequency vibrational spectra of aqueous halides and selected pseudohalides are interpreted in terms of interactions between the anions and the water. A weak band in the isotropic Raman spectrum at *ca.* 200 cm^{-1} originates with the symmetric stretching mode of the $\text{A}^- \cdots \text{HOH}$ species. This assignment is based on experimental studies of aqueous anions in H_2O , D_2O and H_2^{18}O and calculations using a model two body harmonic oscillator comprising one water molecule and the anion. The model is shown to be consistent with quantum mechanics and *ab initio* molecular orbital calculations. The integrity of the model is reaffirmed at high levels of theory and the inclusion of electron correlation in the calculations. An octahedral structure is proposed to reconcile evidence of larger complexes with the observation of only one hydrogen bond on the picosecond time scale of the Raman measurement. It is conjectured that the dynamics of the $\text{A}^- \cdots \text{HOH}$ vibration is influenced by neighbouring molecules.

Acknowledgements

I am greatly indebted to Professor M. H. Brooker for his patient, consistent and inspirational guidance as my research supervisor, and to Drs R. Poirier and P. Tremaine as members of my supervisory committee. Also acknowledged are my fellow graduate students and faculty members in the of the Department of Chemistry and the Department of Physics and several undergraduate students who have assisted with the research.

Assistance from the Department of Computing and Communications and the use of the high performance computing facilities is acknowledged.

Financial assistance was received from Professor Brooker's research funds, the Department of Chemistry and the School of Graduate Studies in the forms of teaching assistantships, departmental support and a graduate research fellowship.

This thesis would not have been possible without the motivation and inspiration from my wife Michelle, her mathematical expertise, support and patience.

Dedication

This thesis is dedicated in the memory of my mother-in-law,

Sarah Fiona Mercer, née Baikie

9 October 1938 - 6 September 1998

Gudip talligenejuk

*et absterget Deus omnem lacrimam ab oculis eorum
et mors ultra non erit neque luctus neque clamor
neque dolor erit ultra quae prima abierunt*

Contents

Abstract	ii
Acknowledgements	iii
Dedication	iv
Table of Contents	v
List of Tables	vii
List of Figures	viii
Symbols and Definitions	ix
1 Introduction	1
1.1 Objectives	3
1.2 The Low Frequency Spectra of Aqueous Electrolytes	4
1.3 Molecular Orbital Calculations	5
1.4 Overview	6
2 Theory	8
2.1 The Linear Harmonic Oscillator	9
2.1.1 The Classical Harmonic Oscillator	9
2.1.2 The Quantum Mechanical Harmonic Oscillator	12
2.1.3 Anharmonicity	16
2.2 Quantum Mechanics of Molecular Systems	18
2.2.1 The Molecular Hamiltonian and Hartree-Fock Theory	18
2.2.2 Molecular Orbitals	21
2.2.3 Post Hartree-Fock Treatments	24
2.2.4 Geometry Optimisation	29
2.2.5 Calculation of Vibrational Frequencies	31
2.2.6 Limitations of the Theoretical Model	34
2.2.7 Solvation Models	35
2.3 Raman Spectroscopy Theory	36
2.3.1 Interaction Between Matter and an Electric Field	36

2.3.2	Interactions Between Matter and Light	38
2.3.3	Time Dependent Quantum Theory	45
3	Instrumentation and Experimental Methods	47
3.1	The Conventional Raman Spectrometer	47
3.2	Chemical Procedures	51
3.3	Treatment of Data	53
4	Experimental and Theoretical Results	54
4.1	Low Frequency Raman Spectra	55
4.1.1	Pure Water and Aqueous Halides	55
4.1.2	Other Anions	61
4.1.3	Isotope Substitution Studies	63
4.1.4	The Influence of Temperature	67
4.1.5	Evaluation of Spectroscopic Parameters	70
4.2	Theoretical Results	73
4.2.1	<i>Ab Initio</i> Molecular Geometries and Energies	73
4.2.2	Normal Mode Force Constants and Frequencies	78
4.2.3	Potential Energy Studies	82
4.2.4	Multiple Hydration and Clusters	85
5	Discussion and Conclusion	91
5.1	Discussion of Experimental Results	91
5.2	Discussion of Theoretical Results	93
	References	99
A	Data Acquisition Code	106
B	Reduced Spectrum and Baseline Calculations	107
C	Example XY Plot File	111
D	Example <i>ab initio</i> Input File	112

List of Tables

3.1	Internal standards	53
4.1	Spectroscopic parameters for the low frequency bands of aqueous halides	72
4.2	Isotopic red shifts	72
4.3	Effect of temperature on the low frequency chloride band . . .	73
4.4	Effect of temperature on the low frequency hydroxide band . .	73
4.5	Optimised structures for water and the anion hydrates	74
4.6	Convergence of parameters by basis set and theory level for chloride monohydrate	78
4.7	Experimental and theoretical frequencies (cm^{-1})	79
4.8	Experimental and theoretical frequencies in H_2O and D_2O . .	81
4.9	Low frequency polarised modes for water clusters calculated at the RHF/6-31+G* level	90

List of Figures

2.1	The linear harmonic oscillator	10
2.2	Slater type and Gaussian type orbitals	22
2.3	Broad and narrow quadratic potential energy surfaces	30
2.4	Light scattering mechanisms	43
3.1	The conventional Raman spectrometer	49
4.1	R_{\parallel} , R_{\perp} and isotropic spectrum of pure water	55
4.2	R_{\parallel} , R_{\perp} and R_{iso} aqueous 0.1 molar $(\text{NH}_4)_2\text{SO}_4$	57
4.3	R_{\parallel} , R_{\perp} and R_{iso} of 5 molar NH_4Cl	58
4.4	Isotropic spectra of 5 molar $\text{NH}_4\text{-I}$, Br, Cl, F and H_2O	60
4.5	Expanded spectra of Fig. 4.4	61
4.6	R_{\parallel} , R_{\perp} and R_{iso} of 5 molar NaOH in H_2O	62
4.7	R_{\parallel} , R_{\perp} and R_{iso} of 5 molal NaCN in H_2O	63
4.8	Isotropic spectrum of 5 molar ND_4Cl in D_2O	64
4.9	Isotropic spectra of 5 molar ND_4Cl in D_2O and NH_4Cl in H_2O	65
4.10	R_{\parallel} for NaOH in H_2O and with ^{18}O substitution	66
4.11	R_{\parallel} for NaOH in H_2O : ^{18}O curve shifted $+7\text{ cm}^{-1}$	67
4.12	Isotropic spectra of NH_4Cl in H_2O at 25, 70 and 150 °C	68
4.13	Isotropic spectra of NaOH in H_2O at 25, 60 and 130 °C	69
4.14	Expanded spectra of NaOH in H_2O at 25, 60 and 130 °C	70
4.15	Parameters of the molecular geometry	75
4.16	<i>Ab initio</i> and Morse potentials for $\text{Cl}^{-}\cdot\text{H}_2\text{O}$	83
4.17	<i>Ab initio</i> potentials for $\text{F}^{-}\cdot\text{H}_2\text{O}$ and $\text{Cl}^{-}\cdot\text{H}_2\text{O}$	84
4.18	Variation of R_{OX} with hydration number for fluoride	87
4.19	Energies of cluster formation versus hydration number	89

Symbols and Definitions

Symbol	Meaning	Value and Units
c	velocity of light in free space	$299792458 \text{ m s}^{-1}$
e	electronic charge	$1.60217733 \times 10^{-19} \text{ C}$
h	Planck's constant	$6.6260755 \times 10^{-34} \text{ J s}$
\hbar	$h/2\pi$	
k	Boltzmann's constant	$1.380658 \times 10^{-23} \text{ J K}^{-1}$
m, m_e	electron rest mass	$9.1093897 \times 10^{-31} \text{ kg}$
m_n	neutron rest mass	$1.6749286 \times 10^{-27} \text{ kg}$
m_p	proton rest mass	$1.6726231 \times 10^{-27} \text{ kg}$
ϵ_0	permittivity of free space	$8.85419 \times 10^{-12} \text{ F m}^{-1}$
μ_0	permeability of free space	$4\pi \times 10^{-7} \text{ H m}^{-1}$

Symbol	Meaning
E	energy, total energy
\mathbf{E}	electric field vector
\mathbf{F}	Fock matrix
\mathbf{F}	force
\hat{H}	Hamiltonian
H_n	Hermite polynomial of order n
I_{\parallel}, I_{\perp}	parallel, perpendicular components of scattered light intensity
J_{ij}	Coulomb integral
K_{ij}	exchange integral
k	force constant
Q	nuclear charge, normal mode coordinate
r	interelectronic distance
R	internuclear distance
R	reduced Raman intensity
\mathbf{S}	overlap matrix
t	time
T	kinetic energy
T	absolute temperature
U, V	potential energy
\dot{x}, \ddot{x}	first and second time derivatives of x
\AA	Angstrom = 10^{-10} m
α	polarisability tensor
β	hyperpolarisability tensor
β	polarisability anisotropy
ϵ	relative permittivity
λ	wavelength
μ	relative permeability, reduced mass
$\boldsymbol{\mu}, \mathbf{p}$	dipole moment
ρ	depolarisation ratio = $I_{\perp} \div I_{\parallel}$
ϕ_{μ}	basis function
ν	frequency in wave numbers ($1 \text{ cm}^{-1} \approx 30,000 \text{ Mc/s}$)
Ψ	time dependent wave function
ψ	wave function
ψ_i	molecular orbital
ω	angular frequency = $2\pi\nu$
∇^2	Laplacian = $\partial^2/\partial x^2 + \partial^2/\partial y^2 + \partial^2/\partial z^2$

Chapter 1

Introduction

When salt dissolves in water, the crystalline structure breaks apart and the salt dissociates into its respective ions. The strong binding forces between the atoms in the crystal are distributed amongst interactions between the ions and the water. Experimental and theoretical studies have shown that there are numerous interactions with a great diversity of lifetimes and relative abundances. One such interaction is that between the negative ion, X^- and water, H_2O . Whereas the interaction between water and the cations is well known, for example Brooker (1986), comparatively little work has been done in the area of understanding the nature of hydration of negative ions. This work is intended to comprise an effort towards completing the understanding of the interaction between salt and water.

In this thesis, a body of evidence for the existence of the $X^- \cdot H_2O$ com-

plex will be presented and examined. The objective is to contribute to an understanding at a fundamental level of the structure of electrolyte solutions that play a central role in the life sciences and many industrial processes. This study is timely in view of the many advances in quantum chemistry.

For almost a century, molecular spectroscopy has been used to probe the structure of matter, particularly as it relates to bonding between atoms. The field expanded rapidly following the pioneering work of Herzberg (1950) and much has become known about chemical bonding as a result. The high frequency region of vibrational spectra, associated with transitions between vibrational states of conventional bonds, has been the subject of considerable investigation. In contrast, the low frequency region, whose signals may originate from intermolecular interactions, has received much less attention in the literature. Modern techniques have facilitated a more detailed analysis of the low frequency region, generally considered to span the frequencies of 3-300 cm^{-1} or about 100-10,000 GHz in the infrared portion of the electromagnetic spectrum. In addition, the assignment of spectral peaks to specific normal modes can be verified and complemented by *ab initio* quantum mechanical methods.

In aqueous systems, conventional infrared spectroscopy is essentially pre-

cluded in this region of the spectrum by the high absorption of energy at these wavelengths by water. Raman spectroscopy on the other hand, uses visible light which is not significantly absorbed by water. Recent developments in digital methods and charged-coupled detectors have revolutionised Raman spectroscopy and a large variety of applications have emerged. For instance, temporal and spatial resolution of Raman spectroscopy are enhanced by the application of digital methods and 180 degree scattering optics coupled with conventional microscopes.

Computational methods have been evolving rapidly and the exponential increase in computing power continues. This has resulted in radical changes in the way computational chemistry is performed. High quality calculations are now easily performed at the undergraduate level and the use of computational methods in chemistry is expected to expand.

1.1 Objectives

In this thesis, the highest frequency and most intense band of the low frequency region of electrolyte solutions will be examined in detail from experimental and theoretical perspectives. The information provided by spectroscopy and molecular orbital calculations will be consolidated and com-

pared by applying the results to a theoretical model. The validity of this model will then be critically examined in the context of developing an understanding of the dynamic structure of anions in solution.

1.2 The Low Frequency Spectra of Aqueous Electrolytes

The low frequency region of aqueous systems is characterised by several broad bands, Nielsen (1993). The most prominent of these have been assigned to the symmetric stretching and bending motions about hydrogen bonds and interactions between the anions and water clusters by Walrafen and Chu (1992). The higher frequency peak for hydroxides was observed at about 290 cm^{-1} and found to be essentially cation independent by Brooker (1986) and Rice (1984), who tentatively assigned this mode to a symmetric stretch about the hydrogen bond between the anion and a water molecule. Earlier X-ray diffraction work by Abu-Dari *et al.* (1978) and Bino and Gibson (1982) have characterised the H_3O_2^- anion as a discrete species in solid complexes. Walrafen (1992) has suggested a multihydrate complex to account for this band in aqueous HCl whereas isotope studies of hydroxides by Brooker (1986) and Rice (1984) provide compelling evidence that the band is due to a hydrogen

bond stretch of the anion hydrate. Anion hydrates have been shown to exist in the gas phase by Arshadi and Kebarle (1970). Considerable work has been done in examining the perturbations of the internal normal modes of water by the presence of hydrogen bonded anions, for example Terpstra *et al.* (1990), but little has been done towards investigating the interactions directly by identifying the low frequency spectral features.

1.3 Molecular Orbital Calculations

The advent of powerful computer technology and advanced parallel processing algorithms has seen the advancement of quantum mechanical calculations of molecular properties to a remarkable accuracy. This has solidified the bridge between theory and experiment, particularly with respect to equilibrium geometries and to vibrational frequency calculations based on molecular force constants deduced from analytical energy gradients (Pople *et al.*, 1979). It is likely that further developments will result in enhanced accuracy of computed values and fewer constraints imposed by approximations, which in the past were required to limit computational costs.

Much of the early work on ion hydration was done by Kistenmacher *et al.* (1973, 1974) who performed small basis set calculations to derive structures

and energies for anion and cation hydrates at several stages of hydration. This was followed by Kollman and Kuntz (1975) who examined fluoride hydration. Over the next two decades, a number of quantum mechanical formalisms were developed and used to study these systems. Density functional theory, (Combariza and Kestner, 1995), and molecular dynamics with *ab initio* perturbation theory, (Xantheas and Dang, 1995), have been exploited to compute thermodynamic properties and potential energy surfaces for anion hydrates.

1.4 Overview

The second chapter of this thesis provides a theoretical background for a model to account for what has been measured and calculated, evidence that the model is applicable to molecular systems and the development of the force constant concept which will ultimately tie theory and experiment. Also in this chapter is a brief outline of molecular orbital theory, the determination of molecular energy, energy gradients, and the use of group theory to determine normal modes, symmetry and vibrational frequencies. The chapter concludes with details on the theory of Raman spectroscopy, the origin and significance of spectral band shape, frequency and polarisation properties.

Chapter 3 deals with the experimental aspects of Raman spectroscopy, the practical implementation of spectroscopic techniques to aqueous systems and the instrumentation of modern spectroscopy. It concludes with an outline of data analysis methods.

The following chapter covers experimental results and describes the observation of a band assigned to the anion-water complex, the isotropic spectra of water and solutions of halides and pseudohalides, deuterated isotopomers, and the effects of temperature on the spectra. Computed results are presented including molecular geometries of the relevant complexes, *ab initio* frequencies, Raman intensities, interaction energies and detailed potential energy diagrams, and a brief presentation of thermodynamic parameters, derived from statistical mechanics.

In the final chapter, the theoretical and experimental results are combined in a complementary fashion. The conclusions drawn from these results are critically examined in the context of the theoretical model and suggestions for further research are formulated.

Chapter 2

Theory

In this section, the theoretical basis for this thesis is established. The harmonic oscillator model is developed and shown to be applicable in describing anion hydration. The harmonic approximation is central to not only the elementary model of molecular vibrations, but also to the calculations of spectroscopic and theoretical vibrational frequencies. Extending the model into the domain of quantum mechanics requires invoking molecular quantum theory to determine force constants between the atoms. These formulations are briefly outlined. The theoretical basis of Raman spectroscopy is introduced, first from a classical perspective and then shown to be consistent with quantum theory through time dependent perturbation theory. Raman spectroscopy provides the essential experimental perspective on which the validity of the theoretical calculations for anion hydration may be assessed.

2.1 The Linear Harmonic Oscillator

A simplistic but useful physical picture of anion hydration is the linear harmonic oscillator. This model can be expected to account for the variations of the vibrational frequency with changes in the strength of the binding force and the mass of the particles engaged in vibrational motion. The essential dynamic features of an anion hydrate may be modelled in accordance with the linear harmonic oscillator with one mass being the water molecule and the other the anion with a hydrogen bond binding the two masses together.

The derivation of the natural vibrational frequency for this system is elementary, but is included to clearly define the model and to provide a starting point from which refinements, such as corrections for anharmonicity and mechanical damping for example, may be developed.

2.1.1 The Classical Harmonic Oscillator

The classical model of the linear harmonic oscillator comprises two bodies separated by an equilibrium distance at which there is no force between them. At separations other than the equilibrium distance, the force operating between two bodies varies in direct proportion to the difference between the actual separation and the equilibrium distance. This is a linear relationship

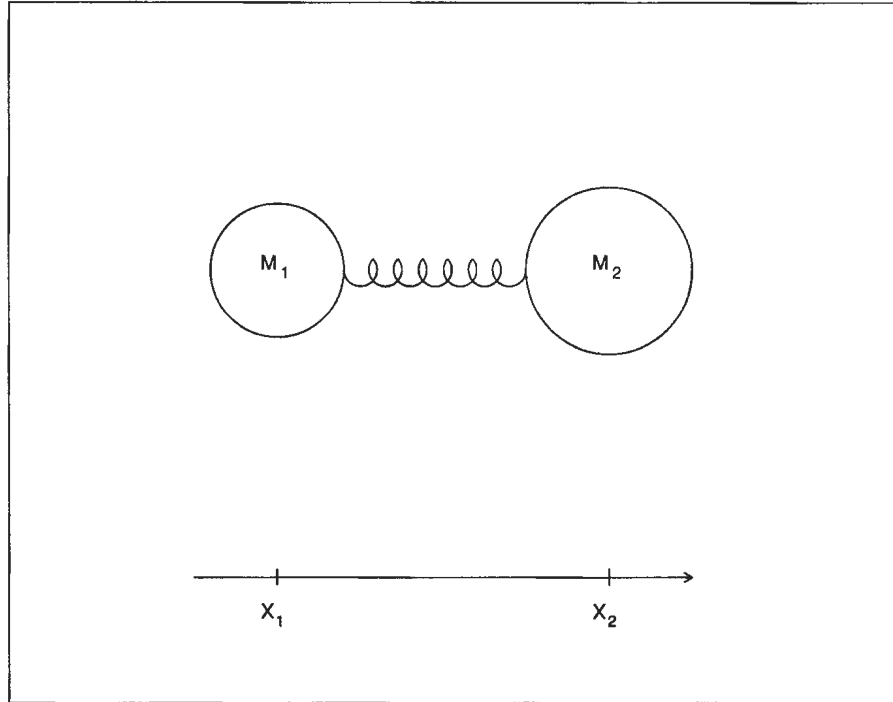


Figure 2.1: The linear harmonic oscillator

and is an expression of Hooke's Law:

$$F = -kx \quad (2.1)$$

where $x = x_t - x_o$ is the difference between the position at time t and the equilibrium position. The geometry and coordinates of this system are shown in Fig. 2.1.

The force F is directed along the x -axis and in the opposite direction as

indicated by the negative sign. By Newton's second law:

$$F = ma = m\ddot{x}$$

and from his third, the equations of motion can be written for each mass:

$$m_1\ddot{x}_1 = k(x_2 - x_1)$$

$$m_2\ddot{x}_2 = -k(x_2 - x_1)$$

These equations exclude any external forces on the system: translation and rotation are not considered as we are concerned only with relative motions along the x -axis. By combining the equations of motion, defining a relative displacement coordinate as $x = x_2 - x_1$ and defining the reduced mass as:

$$\mu = \left(\frac{1}{m_1} + \frac{1}{m_2} \right)^{-1} \quad (2.2)$$

we can write for the equation of motion:

$$\mu\ddot{x} + kx = 0 \quad (2.3)$$

a linear second order differential equation. This admits a periodic solution such as:

$$x = A \sin(\omega t + \phi)$$

Substituting this into Eqn. 2.3, and solving for the angular frequency ω , we obtain:

$$\omega = k^{\frac{1}{2}}\mu^{-\frac{1}{2}} \quad (2.4)$$

that is, the vibrational frequency of a classical harmonic oscillator varies in inverse relation to the square root of the reduced mass of the system for a given force in operation between the two bodies comprising this system.

2.1.2 The Quantum Mechanical Harmonic Oscillator

The fundamental equation in quantum mechanics is the Schrödinger equation:

$$\hat{H}\Psi = i\hbar\frac{\partial\Psi}{\partial t} \quad (2.5)$$

where Ψ is a time dependent wavefunction. In accordance with the postulates of quantum theory and the Heisenberg uncertainty principle, Ψ contains all information which can ever be known about the system it describes. Except under special circumstances, in particular transitions between molecular energy levels, it is satisfactory to separate the Schrödinger equation into its time dependent and time independent components, and consider only the latter, viz.:

$$\hat{H}\psi = E\psi \quad (2.6)$$

E , the energy of the system, is an eigenvalue of the time independent wave function, ψ . In principle, the exact energy can be calculated from this expression once the system eigenfunction has been found. Exact solutions to this equation have been determined for several systems including the hydrogen atom and the harmonic oscillator.

In general, the total energy of a system comprises the kinetic and potential contributions:

$$E = T + V$$

The kinetic component is given by

$$T = \frac{1}{2}mv^2$$

or more generally for a two body system,

$$T = \frac{p^2}{2\mu} \tag{2.7}$$

where μ is the reduced mass as defined by Eqn. 2.2.

From the postulates of quantum mechanics, the operator corresponding to the momentum observable in one dimension is:

$$-i\hbar \frac{d}{dx} \tag{2.8}$$

Eqns. 2.7 and 2.8 combine to give the kinetic term of the Hamiltonian,

$$\frac{-\hbar^2}{2\mu} \frac{d^2}{dx^2}$$

The potential energy operator is the same as the potential energy. This is derived from the force as follows. Because

$$F = -\frac{dV}{dx}$$

and

$$F = -kx$$

we can write for the harmonic oscillator:

$$V = -\int_0^x F dx = \frac{kx^2}{2}$$

Adding the kinetic and potential terms yields the Hamiltonian. This operates on the vibrational wave function, ψ to give the system energy as an eigenvalue. The Schrödinger equation for the linear harmonic oscillator can now be written:

$$\left(\frac{-\hbar^2}{2\mu} \frac{d^2}{dx^2} + \frac{kx^2}{2} \right) \psi = E\psi \quad (2.9)$$

Eqn. 2.9 is a second order differential equation with non-constant coefficients. Its solution comprises a family of eigenfunctions which consist of a normalising factor N_n , Hermite polynomials H_n and a Gaussian function, $e^{-\alpha x^2/2}$ with the general form:

$$\psi_n = \left(\frac{(\beta/\pi)^{\frac{1}{2}}}{2^n n!} \right)^{\frac{1}{2}} H_n(q) e^{-q^2/2} \quad (2.10)$$

where $\beta = \sqrt{\mu k}/\hbar$ and $q = \sqrt{\beta}x$. The eigenvalues are:

$$E_n = \hbar \left(\frac{k}{\mu} \right)^{\frac{1}{2}} (n + 1/2) \quad (2.11)$$

By invoking the Bohr relationship:

$$\Delta E = \hbar\omega$$

and noting that

$$\Delta E = E_{n+1} - E_n$$

we can eliminate E from Eqn. 2.11 to obtain:

$$\hbar\omega = \hbar \left(\frac{k}{\mu} \right)^{\frac{1}{2}}$$

therefore,

$$\omega = k^{\frac{1}{2}}\mu^{-\frac{1}{2}} \quad (2.12)$$

which is the same as the classical relation, Eqn. 2.4.

Although the expression for the vibrational frequency is identical for the classical and quantum harmonic oscillators, the latter has additional physical constraints. By Eqn. 2.11, it is impossible for the system to have zero energy; the minimum energy is $\frac{1}{2}\hbar k^{\frac{1}{2}}\mu^{-\frac{1}{2}}$. This is the zero point energy and the fact that the system cannot be in a zero energy state is consistent with the Heisenberg Uncertainty principle. The zero energy state would require

the kinetic and potential terms to be identically zero. These depend on the momentum and position respectively and because these variables commute, the condition

$$\Delta p \Delta x \geq \hbar/2$$

specifically precludes a zero energy state.

Also by Eqn. 2.11, the energy levels are quantised. It can be further shown that adjacent eigenfunctions are orthogonal, that only specific transitions are possible and that quantum mechanical tunnelling is possible (McQuarrie, 1983).

2.1.3 Anharmonicity

This model can be further refined by making allowances for the convergence of the energy levels near the dissociation limit and by precluding the two bodies touching one another. These features contribute to an asymmetry of the potential function about $R_0 = 0$, ie.: an anharmonicity. When R approaches zero, nuclear repulsion causes the potential to increase very rapidly. As R approaches infinity, the potential approaches zero asymptotically as the particles' interaction diminishes.

The harmonic model is an approximation of a real system. In general it

is reasonably accurate, but there are instances where anharmonic effects can not be neglected. Anharmonicity is expressed as nonlinear terms in the force constant expression:

$$F = -kx - k'x^2 - k''x^3 \dots$$

where k' and k'' are the nonlinear contributions to the force.

The potential associated with a nonlinear force constant is not quadratic and several empirical potentials have been proposed to deal with anharmonic effects. For example, a potential function developed by Morse (1929) has been implemented in the Schrödinger equation and the eigenvalues computed. The Morse and other potentials will be discussed in Chapter 5.

Another deviation from harmonicity is the effect of damping. This can be expressed in the simplest case as a force linearly dependent on the velocity at which the bodies move, ie.:

$$F = -kx - b\dot{x}$$

where b is the damping coefficient. It has been shown, (French, 1971) for example, that the effect of damping is to reduce the amplitude of the vibrations and their frequencies:

$$\omega^2 = \frac{k}{\mu} - \frac{b^2}{4\mu^2} \tag{2.13}$$

It is also seen from this expression that the decrease in frequency caused by damping varies inversely with the reduced mass. Damping of molecular vibrations has been studied by Mizoguchi *et al.* (1992).

2.2 Quantum Mechanics of Molecular Systems

The quantum mechanical harmonic oscillator model cannot be used *a priori* to determine force constants for a real molecule. To calculate these force constants, the postulates of quantum mechanics must be applied to a molecular system. In principle, for a given molecule, a Hamiltonian and wave functions can be expressed in terms of four fundamental constants and used to evaluate the energy, equilibrium structure, vibrational frequencies and many other properties of the molecule.

2.2.1 The Molecular Hamiltonian and Hartree-Fock Theory

An accurate approximation of a Hamiltonian for a molecule can be written by assuming *inter alia*, relativistic and magnetic effects to be negligible, point sizes for the nuclear and electronic charges, and considering only the interactions between pairs of charged species. In atomic units the mass of

the electron and the electrostatic coefficients are unity. The Hamiltonian is:

$$\hat{H} = -\frac{1}{2} \sum_{A=1}^M \frac{\nabla_A^2}{M_A} - \frac{1}{2} \sum_{i=1}^N \nabla_i^2 - \sum_{A,i}^{M,N} \frac{Q_A}{r_{Ai}} + \sum_{i,j>i}^{N,N} r_{ij}^{-1} + \sum_{A,B>A}^{M,M} \frac{Q_A Q_B}{R_{AB}} \quad (2.14)$$

The terms in this expression are the nuclear and electronic kinetic energies, and the nuclear-electron attraction, the electron-electron repulsion, and the nuclear-nuclear repulsion potentials.

Because the masses of nuclei are several orders of magnitude greater than that of an electron, they move much slower and can be considered stationary while computing the electronic energies. This is the basis of the Born-Oppenheimer approximation whereby a partition of the nuclear and electronic contributions to the Hamiltonian is acceptable and the total molecular eigenfunction can be written as a product of the electronic and nuclear eigenfunctions, ie.:

$$\Psi(r, R) = \psi_e(r, R)\psi_N(R)$$

From this, the molecular Schrödinger equation divides into two eigenvalue equations that can be solved independently: a feature that is exploited in the calculation of not only molecular energies, but minimum energy, equilibrium molecular structures. This approximation results in a very modest discrepancy in the calculated energy by a factor of the order of m_e/M_N .

A further simplification is required because we cannot deal exactly with more than two interacting bodies. It is necessary to approximate the interactions between a given electron and the others as a mean potential. This is the Hartree-Fock approximation. The Hartree-Fock method frequently yields results of the required quality and in instances where it does not, it may be used as a first approximation for refinements such as Møller-Plesset perturbation theory (MPPT) and configuration interaction (CI) levels of theory. The formalism is outlined by Szabo and Ostlund (1996) and involves the derivation of a Fock operator $f(1)$ to approximate the electronic Hamiltonian:

$$f(1) = h(1) + \sum_a^{N/2} J_a(1) - K_a(1)$$

Here, the mean potential is expressed by the electrostatic Coulomb integral, $J_a(1)$ and the purely quantum mechanical exchange integral, $K_a(1)$. Contributions to the Fock operator from the core Hamiltonian,

$$-\frac{1}{2}\nabla_1^2 - \sum_{A=1}^M \frac{Z_A}{r_{1A}}$$

are designated $h(1)$. Because each orbital is doubly occupied, the summation is over $N/2$. The Fock operator acts on an orbital to give the Hartree-Fock orbital energy, ε_a ,

$$f\psi_a = \varepsilon_a\psi_a$$

This equation is solved by the self consistent field procedure: an iterative process starting with an initial guess at ψ_a which is used to calculate the mean potential for each electron. An improved value for ψ_a results and this is used to determine the mean field again. This process is repeated until the calculated field converges.

2.2.2 Molecular Orbitals

Examples of accurate wavefunctions for $1s$ and $2p_x$ electrons are Slater atomic orbitals:

$$\begin{aligned}\phi_{1s} &= \left(\frac{\zeta_1^3}{\pi}\right)^{1/2} e^{-\zeta_1 r} \\ \phi_{2p_x} &= \left(\frac{\zeta_2^5}{32\pi}\right)^{1/2} x e^{-\zeta_2 r/2}\end{aligned}$$

where r is the distance of the electron from the nucleus. The accuracy of these orbitals is offset by difficulties in computing their integrals. For this reason, Gaussian functions are used, for example:

$$g_{xx}(\alpha, r) = \left(\frac{2048\alpha^7}{9\pi^3}\right)^{1/4} x^2 e^{-\alpha r^2}$$

As shown in Fig. 2.2, a Gaussian function represents a Slater orbital at intermediate values of x , an arbitrary coordinate. Near the nucleus, $x = 0$, the Gaussian function has too little slope and does not reflect the cusp at $x = 0$. At larger values of x the value of ϕ_i is too small for the Gaussian

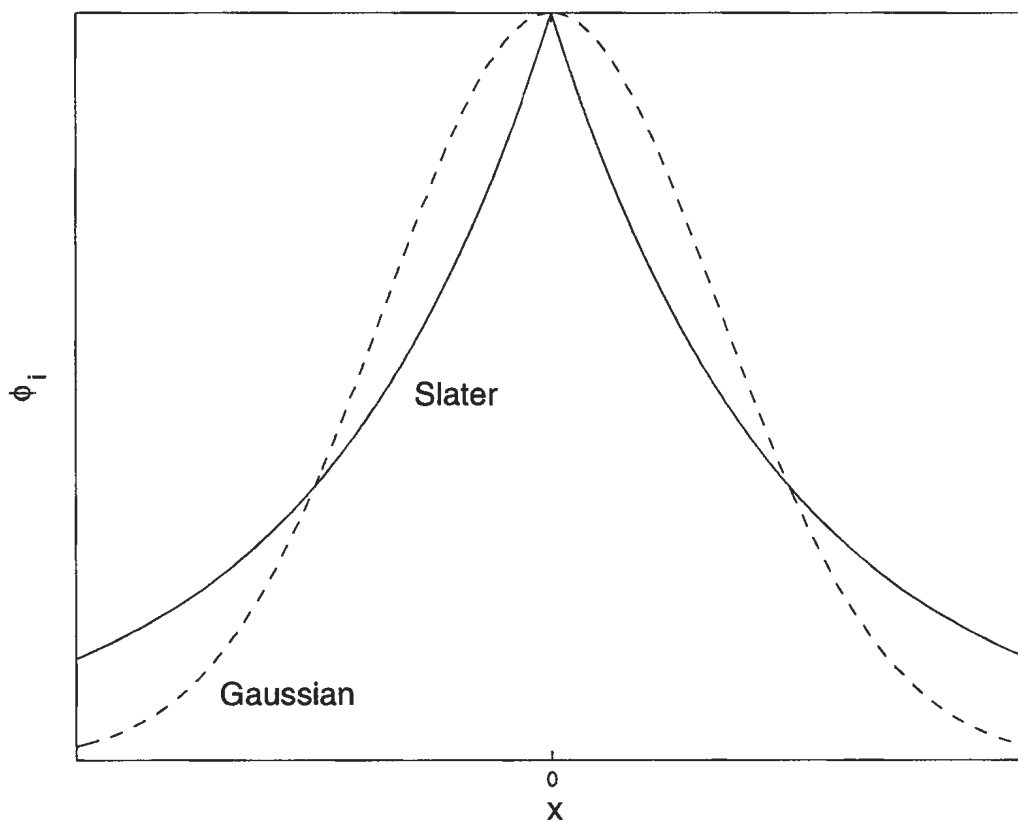


Figure 2.2: Slater type and Gaussian type orbitals

function. It is not possible to adjust the Gaussian coefficients so that the function will approximate all regions of the Slater orbital; this degree of flexibility can only be achieved by using additional Gaussian functions and adjusting their coefficients. In this manner, the atomic (or molecular) orbital is constructed from a linear combination of atomic orbitals (LCAO) which

are simply one-electron basis functions:

$$\psi_i = \sum_{\mu=1}^N c_{\mu i} \phi_{\mu} \quad (2.15)$$

The LCAO coefficients are determined by the variational principle: an approximate wave function for a given system and Hamiltonian will always give an energy that is higher than that obtained if an exact wave function were used. This can be proved as shown by McQuarrie (1983). If the exact energy for a system is E , and we have an approximate eigenfunction ψ expressed as the sum of n basis functions ϕ_n , viz.:

$$\psi = \sum_n c_n \phi_n$$

Then by the Schrödinger equation,

$$E_{\psi} = \frac{\sum c_n^* c_n E_n}{\sum c_n^* c_n}$$

is the approximate energy. The difference between this and the exact energy

is:

$$E_{\psi} - E_o = \frac{\sum c_n^* c_n (E_n - E_o)}{\sum c_n^* c_n}$$

and because

$$c_n^* c_n > 0$$

then

$$E_\psi > E_o$$

Hence the approximate eigenfunction yields an energy that is always an upper limit of the exact energy. The problem now becomes determining ψ such that its energy eigenvalue is a minimum. This is accomplished by determining the expansion coefficients $c_{\mu i}$ of Eqn. 2.15 by the Roothan Hall matrix equation:

$$\sum_{\nu=1}^N (\mathbf{F}_{\mu\nu} - \varepsilon_i \mathbf{S}_{\mu\nu}) c_{\nu i} = 0 \quad \mu = 1, 2, \dots, N$$

In this expression, \mathbf{S} is the overlap matrix, related to the relative spatial position of the orbitals and \mathbf{F} is the Fock operator matrix. From the expansion coefficients, an electron density matrix \mathbf{P} can be determined. \mathbf{P} and \mathbf{F} are interdependent so that the equations must be solved iteratively until \mathbf{P} converges, i.e., it becomes self-consistent (Szabo and Ostlund, 1996). The procedure uses Slater determinants to ensure that the resultant orbitals are orthogonal as required by the Pauli principle.

2.2.3 Post Hartree-Fock Treatments

The accuracy of the wave function, and the eigenvalue that is calculated from it, depends on the size of the basis set. The Hartree-Fock limit is the lowest variational energy that can be obtained with the SCF procedure, regardless

of the size of the basis. Frequently, systematic empirical corrections can be applied to improve results but post Hartree-Fock methods are required if energy accuracies of better than a few percent or properties dependent on electron correlation are desired. Configuration Interaction and Perturbation Theory can be used to improve Hartree-Fock calculations.

Hartree-Fock theory can be made more flexible to deal with open shell systems by using unrestricted spin extension, but neither this nor restricted Hartree-Fock theory can completely describe electron correlation because of the Fock operator does not include all the correlation terms. The Hartree-Fock approximation is no longer acceptable in dealing with systems where electron correlation is important, for example in describing dissociation. Refined methods of *ab initio* calculations have been developed to deal with these systems.

Perturbation Theory

In perturbation theory, the exact Hamiltonian is expressed as a sum of a known term $\hat{H}^{(0)}$ and a perturbation, V :

$$\hat{H} = \hat{H}^{(0)} + V$$

Møller-Plesset Perturbation Theory (MPPT) assigns the sum of one electron Fock operators to $H^{(0)}$ and the effects of electron correlation to V .

The formalism for MPPT is implemented by expanding the wave function as a series in orders of λ :

$$\psi_\lambda = \psi^{(0)} + \lambda\psi^{(1)} + \lambda^2\psi^{(2)} + \dots$$

or, in the notation of Dirac:

$$|n\rangle = |n^{(0)}\rangle + \lambda|n^{(1)}\rangle + \lambda^2|n^{(2)}\rangle + \dots$$

Similarly, for the energy eigenvalues,

$$E_\lambda = E^{(0)} + \lambda E^{(1)} + \lambda^2 E^{(2)} + \dots$$

where

$$\hat{H}^{(0)}|n^{(0)}\rangle = E^{(0)}|n^{(0)}\rangle$$

is the unperturbed Schrödinger equation. This relation is applied to the higher terms in the expansions. Expressions are derived for the n order wave function, which are used to determine an $n+1$ order correction to the energy, i.e.,

$$E_n^{(1)} = \langle n^{(0)}|V|n^{(0)}\rangle$$

and

$$E_n^{(2)} = \langle n^{(0)} | V | n^{(1)} \rangle$$

where

$$\langle n | V | n \rangle = \int_{-\infty}^{\infty} \psi^* V \psi d\tau$$

The resultant energy is the sum of the unperturbed energy, and a series of n -order corrections in terms of the $n - 1$ order wavefunctions.

Although perturbation theory is not variational, it is size consistent and can give better energy calculations for molecular interaction energies. Perturbation theory is also used in the quantum treatment of the interaction between matter and radiation.

Configuration Interaction

Another way to partially overcome the deficiencies of the Hartree-Fock approximation is to include more than one determinant in the wave function. This allows the wave function to include the effects of correlation between electrons of opposite spin by including determinants for other electron configurations. The number of configurations included in the wave function can be increased until the calculations of the desired quality is obtained. Single

configuration includes only one expansion term, viz.:

$$\psi = a_0\psi_0 + \sum_i^o \sum_a^v a_i^a \psi_i^a$$

The inclusion of single and doubles yields a wave function which contains the additional terms

$$\sum_{i<j}^o \sum_{a<b}^v a_{ij}^{ab} \psi_{ij}^{ab}$$

and so on. Because the CI wavefunction has more variational coefficients the CI energy is lower than that calculated by the HF method. The difference, in terms of the orbitals, is a portion of the electron correlation energy. Higher levels of CI can be used to evaluate more of the correlation energy up to the nonrelativistic limit. A problem with lower levels of CI is the lack of size consistency. This can lead to errors in the energy calculated for reactions where two or more molecules combine.

Density Functional Theory

Another level of theory calculation that better incorporates electron correlation is Density Functional Theory (DFT), (Kohn, 1965). Becke (1989) and Pople (1992) have contributed significantly to DFT in chemical applications. DFT also includes components of the energy from the exchange integral that are not included at the Hartree-Fock level. Unlike HF which

deals with electrons, DFT uses electron density. This simplifies the problem computationally at a fair to modest cost in terms of accuracy.

2.2.4 Geometry Optimisation

Once satisfactory wave functions have been obtained, the total energy of the molecule and its gradients can be determined and used to find a molecular geometry. Again, this is an iterative process whereby the geometry is adjusted to reduce the total energy, the SCF procedure is repeated and a corresponding value for the total energy is calculated. The process is repeated until the energy gradient with respect to each nuclear coordinate is reduced to a predetermined value. There are various methods for this procedure, some of which involve the calculation of second derivatives as a means of improving the efficiency.

The geometry corresponding to the threshold of convergence of the energy is taken to be the equilibrium geometry. Normally, this threshold is taken to be 10^{-5} but the presence of weakly interacting parts of a molecule may require a tighter threshold. The potentials about a given coordinate, such as bond stretching or angular torsion, are shown in Fig. 2.3. For a given arbitrary threshold value at some small value above the potential energy axis, the broad potential will have a greater range of coordinate that satisfies the

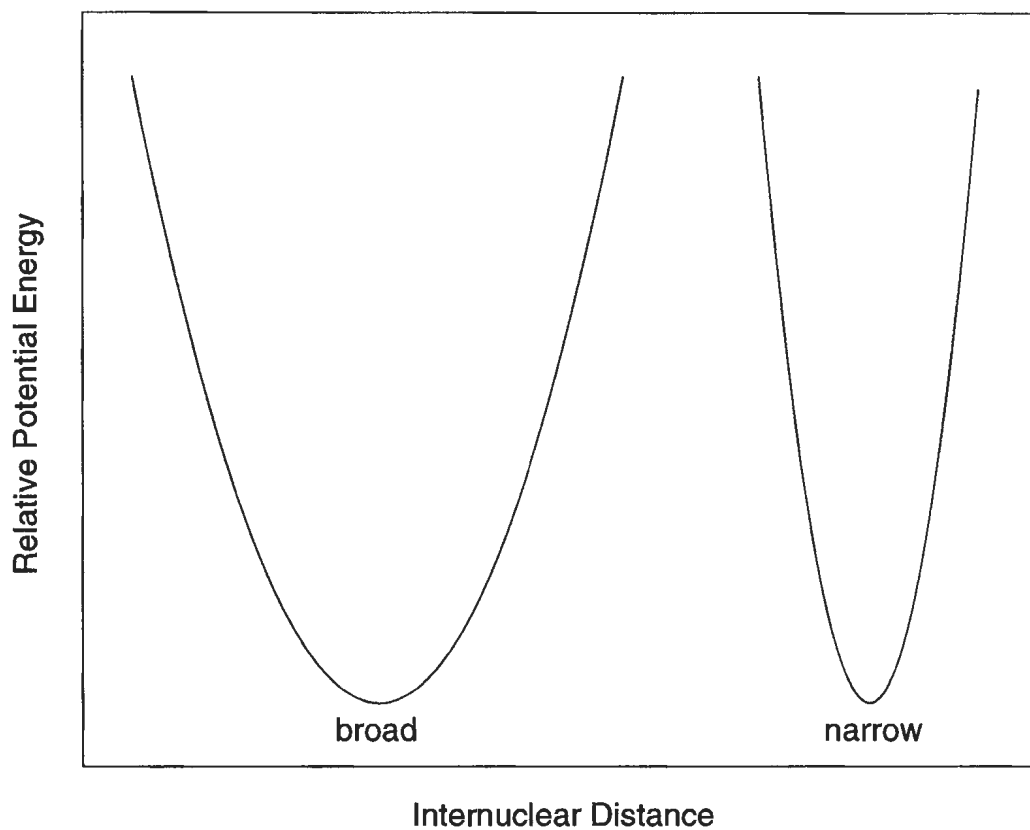


Figure 2.3: Broad and narrow quadratic potential energy surfaces

threshold than the narrow potential. A more constrained threshold value is therefore required to adequately determine the weaker interactions.

Another criterion for the equilibrium geometry is that all force constants between the nuclei are positive. A negative force constant will lead to an imaginary (non-real) vibrational frequency and indicates that the optimisation has terminated at a transition state on the potential hypersurface.

This corresponds to a non-global minimum such as a saddle point and a non-equilibrium geometry.

Geometry optimisation is important to the evaluation of force constants for another reason. As will be shown in the next section, the accuracy of the theoretical force constants is limited by how close the calculated geometry is to the equilibrium configuration.

2.2.5 Calculation of Vibrational Frequencies

The energy and its gradients as calculated by *ab initio* methods can now be employed to compute force constants. These lead directly to vibrational frequencies by Eqn. 2.4. Using the linear two-body oscillator described earlier, an infinitesimal change in the relative position of the two bodies, dx will cause a change in the potential energy of the system given by:

$$dV = -Fdx$$

For a linear force, for example, Eqn. 2.1,

$$dV = kxdx$$

This is integrated to obtain the potential:

$$V = \int_{x_0}^{x_1} kxdx = \frac{1}{2}k(x_1 - x_0)^2 + V_0$$

or

$$V = V_o + \frac{1}{2}kx^2 \quad (2.16)$$

Expanding an arbitrary potential as a Taylor Series about $x = x_o$:

$$V = V_{x=x_o} + \left(\frac{dV}{dx}\right)_{x=x_o} x + \frac{1}{2!} \left(\frac{d^2V}{dx^2}\right)_{x=x_o} x^2 + \frac{1}{3!} \left(\frac{d^3V}{dx^3}\right)_{x=x_o} x^3 + \dots$$

This can be rewritten as:

$$V = V_o + \frac{1}{2}kx^2 + \frac{1}{6}k'x^3 + \dots \quad (2.17)$$

Comparing Eqns. 2.16 and 2.17 allows us to equate the second derivative of the potential energy with the force constant, provided *the derivative is taken at the equilibrium position and the force is harmonic*. These constraints assure that the first, third and higher order derivatives in the expansion are negligible so that it simplifies to the quadratic form of Eqn. 2.16.

This treatment is easily extended into three dimensions and, with the aid of group theory, over all normal modes a molecule. Hehre *et al.* (1986), who have done much work in combining group theory and *ab initio* calculations, start by expressing the classical total energy as the sum of the kinetic and potential energies:

$$E = T + V = \frac{1}{2}mv^2 + V$$

For an N-atom molecule with an equilibrium potential V_{eq} ,

$$E = \frac{1}{2} \sum_{i=1}^{3N} \dot{q}_i^2 + V_{eq} + \frac{1}{2} \sum_{i=1}^{3N} \sum_{j=1}^{3N} \left(\frac{\partial^2 V}{\partial q_i \partial q_j} \right)_{eq} q_i q_j \quad (2.18)$$

where the q_i are mass weighted coordinates according to

$$q_i = M_i^{1/2} (x_i - x_{i,eq})$$

and

$$\ddot{q}_i = - \sum_{j=1}^{3N} f_{i,j} q_j \quad j = 1, 2, \dots, 3N$$

The harmonic force constants are:

$$f_{ij} = \left(\frac{\partial^2 V}{\partial q_i \partial q_j} \right)_{eq}$$

This is analogous to the second derivative in the expansion shown earlier.

Both numerical and analytical differentiation have been used to evaluate these derivatives. Although the numerical method may have problems with rounding errors in certain instances, analytical derivatives are complicated to implement, but work by Pople *et al.* (1979) has made it possible to do so at some of the higher theory levels.

The determination of the 3N force constants leads directly to the normal mode vibrational frequencies by Eqn. 2.4. Six of the normal mode frequencies (or five in the case of linear molecules) will be zero as they correspond to translation or rotation of the entire molecule.

2.2.6 Limitations of the Theoretical Model

The Hartree-Fock theoretical frequencies are generally about 10 percent too high when compared with the experimental values. This error is reduced to about 5 percent at the Møller-Plesset level. These discrepancies are largely systematic and empirical methods have evolved to correct them as described by Hehre *et al.* (1986).

Derivatives can be calculated of the dipole moments and polarisabilities to determine theoretical IR and Raman activities, (Svendsen, 1979), although these are still limited in their ability to reproduce experimental results, (Yamaguchi *et al.*, 1986). At this time, post Hartree-Fock intensities and depolarisations calculations are unavailable.

Basis set superposition error arises when dealing with clusters of molecules because the cluster uses more basis functions in describing the wave function than the isolated molecules. As a result, the cluster association energy is overestimated. Pye *et al.* (1994) have evaluated BSSE for several systems and have concluded that the BSSE of hydrated systems is of the order of 1 kJ mol⁻¹ for moderate to large basis sets. Their work did not include anions and a study of diffuse functions on the BSSE but it can be assumed that the 1 kJ mol⁻¹ figure will not be significantly altered. The magnitude of the

error does not change appreciably as moderate basis sets are made larger which is the case when diffuse functions are incorporated in the basis.

2.2.7 Solvation Models

Concentrated aqueous solutions are required to obtain satisfactory Raman spectra, hence solute-solute and solvent-solvent effects have the potential to influence the spectra. In addition, *ab initio* calculations are done on isolated species and not bulk solutions so the extent to which these calculations can describe aqueous systems is inherently limited. Work has been done in the area of supplementing *ab initio* calculations with solvation effects by invoking the Onsager reaction field theory. Wong *et al.* (1991) have used this method to calculate changes in molecular geometry and charge distributions as a result of the presence of a solvation reaction field. In a subsequent study, Wong *et al.* (1992) described strong solvent effects on molecular properties. Of particular interest was a solvation model calculation of the vibrational frequencies of sulphamic acid in a dielectric with a relative permeability of 40. These were generally about 50 cm^{-1} lower than the corresponding gas phase calculations.

This improved agreement between experimentally measured and theoretical vibrational frequencies is encouraging, but Foresman *et al.* (1996), have

noted that many arbitrary choices are still required in specifying parameters for solvation models. Further theoretical work in this area is directed towards improving the incorporation of solvation effects into these calculations.

2.3 Raman Spectroscopy Theory

2.3.1 Interaction Between Matter and an Electric Field

If a molecule with a permanent dipole moment is subject to a uniform and static electric field E , the molecule will respond by reorienting so as to minimise its potential energy

$$V = -\mu E \cos \theta$$

where μ is the dipole moment and θ is the angle subtended by the field and the dipole. For an ensemble of molecules the combined effect of the molecular dipole moments can be found from Boltzmann statistics, (Brand and Speakman, 1960):

$$\bar{\mu}_o = \frac{\mu \int e^{-V/kT} \cos(\theta) d\theta}{\int e^{-V/kT} d\theta} \quad (2.19)$$

The quotient is a normalising factor so that $\bar{\mu}_o$ is the average dipole moment per molecule. By invoking trigonometric identities and noting that $\mu E/kT$ is small, Eqn. 2.19 can be simplified to:

$$\bar{\mu}_o = \frac{\mu^2}{3kT} E = \alpha E$$

The relationship between the net dipole moment and the applied electric field is linear and the coefficient, $\mu^2/3kT$ is the polarisability, α . Because the polarisability generally depends on the orientation of the molecule with respect to the applied field it is a tensor. An intense electric field causes the dipole moment to exhibit a nonlinear response denoted by the hyperpolarisability tensor, β . The dipole moment in vector notation is:

$$\boldsymbol{\mu} = \boldsymbol{\mu}_{E=0} + \frac{1}{2}\boldsymbol{\alpha}\mathbf{E} + \frac{1}{6}\boldsymbol{\beta}\mathbf{E}^2 + \dots$$

Hyperpolarisability, though normally neglected in Raman spectroscopy, can contribute to nonlinearity.

The dipole moment has static and induced components:

$$\boldsymbol{\mu} = \boldsymbol{\mu}_o + \boldsymbol{\mu}_i \tag{2.20}$$

and the total dipole moment is related to the dielectric constant by the Debye-Langevin equation,

$$(\epsilon_o - 1)\frac{M}{d} = 4\pi N_A \left(\bar{\alpha} + \frac{\mu^2}{3kT} \right)$$

This relation links the spectroscopic polarisability and optical properties such as refractivity to the bulk properties of a material by way of its dielectric constant. Related equations are exploited in the development of solvation models.

2.3.2 Interactions Between Matter and Light Scattering Geometry

Electromagnetic radiation of which light is an example, comprises three mutually orthogonal electric, magnetic and propagation vectors. The electric and magnetic vectors fluctuate sinusoidally in space and time. The interaction of the electric component of the radiation with matter can cause an induced dipole moment μ_i in addition to the permanent dipole moment, μ_o that may be present in accordance with Eqn. 2.20 with the exception that the induced component is now time dependent and can be further resolved into contributions from each of the normal vibrational modes Q_i . Hence

$$\mu_i = \sum_i^{3N-6} \frac{\partial \mu}{\partial Q_i} Q_i$$

for an N atom molecule.

The dependence of dipole moment on polarisability means that the total polarisability can be expanded in terms of the normal modes in the analogous expression:

$$\alpha = \sum_i^{3N-6} \frac{\partial \alpha}{\partial Q_i} Q_i$$

As the axes of polarisability and exciting light are not generally parallel, the polarisability must be expressed as a tensor:

$$\boldsymbol{\alpha} = \begin{pmatrix} \alpha_{xx} & \alpha_{xy} & \alpha_{xz} \\ \alpha_{yx} & \alpha_{yy} & \alpha_{yz} \\ \alpha_{zx} & \alpha_{zy} & \alpha_{zz} \end{pmatrix}$$

This has symmetric and anisotropic components:

$$\alpha = \frac{1}{3}(\alpha_{xx} + \alpha_{yy} + \alpha_{zz}) \quad (2.21)$$

and

$$\beta = \frac{1}{2} \left((\alpha_{xx} - \alpha_{yy})^2 + (\alpha_{yy} - \alpha_{zz})^2 + (\alpha_{zz} - \alpha_{xx})^2 + 6(\alpha_{xy}^2 + \alpha_{yz}^2 + \alpha_{zx}^2) \right)^{\frac{1}{2}}$$

respectively. The coordinates of the polarisability tensor can always be transformed such that the cross terms in the anisotropy become zero. The anisotropy can be written as:

$$\beta = \frac{1}{2} \left((\alpha_{xx} - \alpha_{yy})^2 + (\alpha_{yy} - \alpha_{zz})^2 + (\alpha_{zz} - \alpha_{xx})^2 \right)^{\frac{1}{2}} \quad (2.22)$$

Eqn. 2.22 is identified with the depolarised component of scattered light whereas the magnitude of the symmetric component relates to intensity of the isotropic component.

The interaction of the electric field component of the radiation must produce a change in dipole moment that is perpendicular to the propagation vector of the incident light. This is because the electric vector, which causes the change, is also at right angles to the propagation vector. Light scattered

at right angles must therefore be polarised. Because the polarisability ellipsoid is not always spherical, the scattered light often has some degree of depolarisation. The isotropic and anisotropic components of scattered light are derived from the experimentally measured polarised and depolarised scattered light intensities:

$$I_{\beta} = I_{\text{aniso}} = I_{\text{dep}} = I_{\perp} \quad (2.23)$$

$$I_{\alpha} = I_{\text{iso}} = I_{\parallel} - \frac{4}{3}I_{\perp} \quad (2.24)$$

The ratio of these intensities, the depolarisation ratio

$$\rho = I_{\perp}/I_{\parallel} \quad (2.25)$$

is less than $\frac{3}{4}$ for a vibrational mode that is symmetric.

Frequencies, Band Shapes and Intensities

Light may be scattered in several ways such as Fluorescence, elastic Rayleigh, inelastic Rayleigh Brillouin, Stokes and anti-Stokes mechanisms. The latter results in light at a higher frequency than the incident whereas the Stokes scattered light is at a lower frequency. The Stokes and anti-Stokes light are sought in Raman spectroscopy and are, in a classical sense, the result of the modulation of the exciting frequency by another frequency, such as a molecular rotation or a normal mode vibration. The composite signal

contains the exciting frequency, the modulating frequency and their sums and differences. This can be shown as follows. The electric intensity of the excitation light of frequency ω_e is at any time, t can be written:

$$E(t) = E_o \sin(\omega_e t)$$

where E_o is the peak intensity. Because

$$\mu_i = \alpha E$$

the dipole moment at any time t is

$$\mu(t) = \alpha E_o \sin(\omega_e t)$$

A molecular vibration at frequency ω_v will cause a modulation of the molecular polarisability with some amplitude F proportional to the change in polarisability with the change in the normal coordinate of the vibration:

$$\alpha(t) = \alpha_o + F \sin(\omega_v t)$$

so that the combined effect on the dipole moment is a product of the two sinusoidal components. That is :

$$\mu(t) = \alpha_o E + F \sin(\omega_v t) E_o \sin(\omega_e t)$$

Expanding this as a product of two sines, $\sin a \sin b = \frac{1}{2} [\cos(a - b) - \cos(a + b)]$ reveals two new frequencies:

$$\mu = \alpha_o E_o \sin(\omega_e t) + \frac{1}{2} F E_o [\cos((\omega_e - \omega_v)t) - \cos((\omega_e + \omega_v)t)]$$

These frequencies are above and below the exciting line ω_e by an amount equal to the molecular vibrational frequency ω_v with ω_e being the exciting wave or Rayleigh line, $\omega_e - \omega_v$ the Stokes frequency and $\omega_e + \omega_e$ the anti-Stokes frequency. This classical model cannot account for the observation that the Stokes intensity is greater than that of the anti-Stokes. This explained by the quantisation of vibrational molecular energy states, as shown in Fig. 2.4. Because the upper vibrational state is less populated than the lower, fewer transitions occur from the upper to lower than *vice versa* and the intensity corresponding to these transitions is lower. The Rayleigh line is the most prominent feature by several orders of magnitude.

Rotational modes which cause a change in the molecular polarisability can also give rise to Raman transitions. These can be observed for gas phase molecules under high resolution. The composite spectrum consists of peaks associated with vibrational and rotational transitions that may give rise to the familiar O, P, Q, R and S branches in the spectra.

The shape of a Raman band is related to the lifetime, nature and environ-

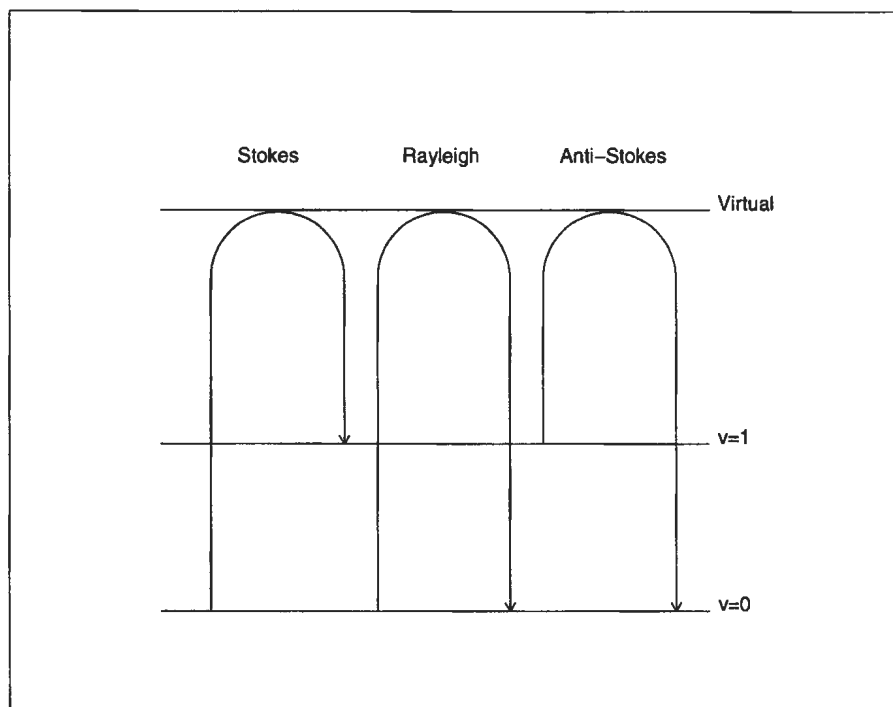


Figure 2.4: Light scattering mechanisms

ment of the particular excited vibrational state. Homogeneous broadening generally imparts a Lorentzian shape to the band and results from a molecule radiating over a range of frequencies. The more predominant inhomogeneous broadening arising from Doppler effects due to a distribution of molecular velocities in non-condensed states, generates a Gaussian shape.

The intensity of the Raman scattered light varies not only with the change in polarisability as the molecule vibrates or rotates, but also with the fourth

power of the frequency and the temperature. The latter is a consequence of the Boltzmann distribution law. If the first vibrational state has a frequency ν then the fraction of molecules in the ground vibrational state is given by

$$1 - e^{-h\nu/kT}$$

where T is the absolute temperature. At room temperature with $\nu = 170 \text{ cm}^{-1}$ for instance, this fraction is less than 50 percent so most of the molecules will be in the excited state. Temperature therefore has a marked effect on the low frequency spectra.

Combining these factors leads to a normalised intensity for the Stokes scattered light, the reduced intensity:

$$R_Q = I(\bar{\nu})\nu_i(\bar{\nu}_o - \bar{\nu}_i)^{-4}(1 - e^{-hc\bar{\nu}_i/kT}) \quad (2.26)$$

which is directly proportional to the number of molecules giving rise to the scattered light. Eqn. 2.26 has been shown to have a solid experimental and theoretical foundation (Brooker *et al.*, 1988; Murphy *et al.*, 1989). Spectra presented in this format are independent of the instrument and the intensity of the exciting line.

2.3.3 Time Dependent Quantum Theory

The application of quantum theory to the interaction between matter and an electromagnetic field invokes the time dependent formalism of Eqn. 2.5. Because the molecular Hamiltonian, Eqn. 2.14, is independent of time and the presence of electromagnetic radiation, it cannot be used in Eqn. 2.5. As outlined by Simmons and Nichols (1997), these dependencies are invoked in Eqn. 2.14 by replacing the momentum operators for the nuclear and electronic kinetic terms by time, spatial and frequency dependent vector potential terms. This creates additional terms in the molecular Hamiltonian. Eqn. 2.5 can then be solved by treating the Hamiltonian as the sum of a time independent component and a component \hat{H}_{int} describing the interactions by time dependent perturbation theory.

$$\left(\hat{H}^0 + \hat{H}_{int}\right) \Psi = i\hbar \frac{\partial \Psi}{\partial t} \quad (2.27)$$

This gives rise to electric dipole transition moments and magnetic transition moments from which transition rates between molecular states may be calculated. These calculations are based on the long wavelength approximation $\lambda \gg R_{AB}$ for the wavelength of light used in spectroscopy and any typical nuclear separations.

The quantum mechanical treatment leads to the formulation of vibro-electronic transition rules and accounts for violation of these rules by the Franck-Condon principle. Line shapes, widths, correlation functions, and other spectroscopic features have been defined in terms of quantum theory. However, like the classical method, the quantum approach still draws on the harmonic approximation.

Chapter 3

Instrumentation and Experimental Methods

3.1 The Conventional Raman Spectrometer

The essential components of a modern Raman spectrometer comprise an intense source of coherent, monochromatic and polarised light, a suitably contained sample and a means to measure the intensity of the scattered light as a function of its wavelength and scattering geometry.

Lasers are almost always used as the light source. They provide light which is constrained to a very narrow band of wavelengths, is coherent and usually polarised. Polarised light is useful in studies of molecular symmetry. Laser lines may be chosen to mitigate problems associated with sample colour and fluorescence.

Because visible light is used in Raman spectroscopy, sample cells need

not be transparent at infrared (IR) wavelengths as is the case with IR spectroscopy. Cells should be inert with respect to the sample as contamination may result if the cell decomposes. This could present a source of interference in the spectra. Fused quartz cuvettes are often used, but are susceptible to dissolution by molten salts and concentrated solutions of fluorides and hydroxides. Sapphire and windowless cells may be used at elevated temperatures with highly caustic samples or molten salts, respectively. Raman spectra can be obtained on a much broader range of samples than for IR spectra. Samples need only be in a form that is reasonably transparent or translucent, and preferably colourless.

A conventional Raman spectrometer is shown in Fig. 3.1. Light from the laser is passed through a filter to remove spurious emissions such as plasma lines. A half-wave plate is used to maintain or rotate the polarisation parallel to the Z axis. The light is then focussed by a lens into the sample which may be heated by a furnace or cooled for temperature studies. An objective lens focuses the light scattered in the Y direction into the monochromator. Polarisation studies are achieved by inserting a polaroid film before the slit. This film is oriented so that light parallel to the Z axis is passed to measure the polarised intensity, denoted $I[X(ZZ)Y]$ and rotated 90° to pass the light

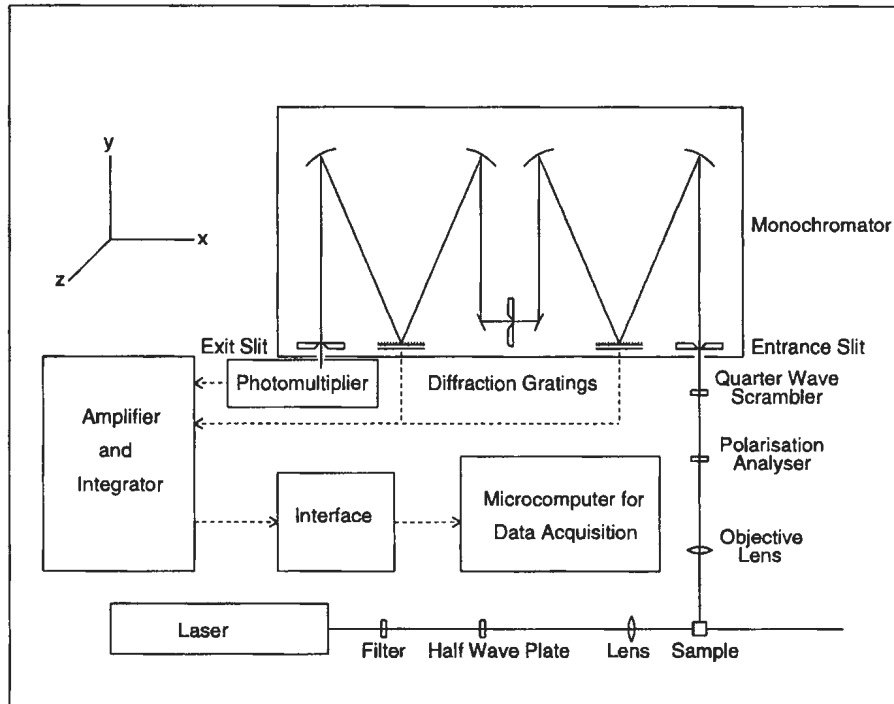


Figure 3.1: The conventional Raman spectrometer

parallel with the X axis for depolarised intensity, $I[X(ZX)Y]$. A quarter wave scrambler in the light path compensates for the dependence of the diffraction gratings on polarisation. Adjustable optical slits are used to optimise the sensitivity and resolution. A double grating unit is shown, but triple grating instruments are often used to remove stray light and sometimes to improve the resolution. The gratings disperse the light so that only a narrow band of frequencies is passed through the slits and into the detector. Because the

dispersion depends on the angle of the grating with respect to the light beam, the centre frequency of the light passing the exit slits can be calibrated in terms of this angle. In this manner, the monochromator acts as a narrow and variable frequency band-pass filter.

Light leaving the monochromator exit slit enters a photomultiplier tube. This device exploits the photoelectric effect whereby an incident photon causes the ejection of an electron from a metal surface. This is followed by several stages of photomultiplication when the electron is accelerated by an applied potential towards an anode, causing secondary emission of about five times as many electrons per stage. Stages are cascaded to produce a multiplication factor of 10^6 . Electrons can also be thermally excited and this will cause a background noise in the signal known as the dark current. This is reduced by cooling the photomultiplier tube to -30°C with a liquid nitrogen heat exchanger.

Current from the photomultiplier is then measured over a specified time interval by a black-box integrator. Integrated counts are obtained at intervals of one half wavenumber as scanned by the monochromator. Spectra are scanned at the rate of $50\text{ cm}^{-1}\text{s}^{-1}$ and the integrator sampled at 0.5 cm^{-1} intervals. The binary coded decimal output of the black box was coupled to

the asynchronous serial port of a microcomputer. Data were recorded with an acquisition routine (Appendix A).

Spectra were obtained using a dual grating Coderg PHO Raman spectrometer. Samples were excited with a Coherent argon ion laser with 1.0 watt output at 514.5 nm. The 488.0 nm line was used for some measurements. Entrance and exit slits were set to obtain a bandwidth of 4 cm^{-1} . A sharp band-pass filter was used to remove plasma lines and other spurious emissions from the laser light. The monochromator was calibrated to within 0.2 cm^{-1} against the laser plasma lines. Calibration of the instrument for the depolarisations was achieved by measuring the intensities of light scattered at both geometries by spectral grade carbon tetrachloride. Except as indicated, all spectra were taken at room temperature, nominally $25\text{ }^{\circ}\text{C}$. A thermostated furnace was used to obtain spectra at higher temperatures.

3.2 Chemical Procedures

Solutions were prepared with triple-distilled water. Water distilled in a glass still was not suitable because its spectrum contained a weak polarised band at 880 cm^{-1} . This band was absent in water that was both distilled and deionised. A small quantity of metallic zinc was added to the ammonium

iodide solution to prevent oxidation of iodide to I_2 and the formation of the coloured I_3^- complex.

Traces of organic material often remain in solid salts as a result of the crystallisation methods used during their production. These impurities can cause fluorescence that distorts the baseline signal and raises noise level by creating a broad background interference. Fluorescent material was removed by treating the solution with activated charcoal, followed by vacuum filtration through a fine glass frit. Samples were contained in sealed quartz cuvettes which had been soaked for several days in dilute sodium hydroxide and thoroughly rinsed with distilled and deionised water. Cuvettes were deemed to be clean when the water flowed smoothly and evenly over walls of the cell without forming droplets. Analytical grade $(NH_4)_2SO_4$, NH_4NO_3 , $NaClO_4 \cdot H_2O$ and $HClO_4$ at a concentration of $0.10 \text{ mol} \cdot \text{L}^{-1}$ were used as internal standards. These were selected because of their low Raman isotropic activity in the $30\text{-}300 \text{ cm}^{-1}$ band and their clearly defined ν_1 peaks. These peaks provided a means of frequency calibration and intensity standardisation. They are stable in aqueous solution and are unlikely to form complexes. The frequencies of the ν_1 peaks for these standards are given in Table 3.1

Table 3.1: Internal standards

Standard	ν_1 Frequency (cm ⁻¹)
ClO ₄ ⁻	930
SO ₄ ²⁻	980
NO ₃ ⁻	1050

3.3 Treatment of Data

Several spectra can be taken and averaged to improve the signal to noise ratio by a factor of \sqrt{n} for n spectra averaged. The intensities of 3 to 6 spectra in the [X(ZZ)Y] and [X(ZX)Y] geometries were averaged to obtain a satisfactory signal to noise ratio. This was followed by two iterations of a three-point Savitsky-Golay smoothing procedure. The intensities were then normalised for the Boltzmann occupancy of states and the fourth power dependence of scattering intensity, Eqn. 2.26. This yielded a flat baseline which was subtracted as a constant offset from each spectrum. The isotropic intensities were calculated for each frequency in accordance with Eqn. 2.24. These routines were uniformly applied to each spectrum with the computer code listed in Appendix B. Commercial computer packages were used to perform spectral deconvolution and fitting of a model curve to the experimental data by least squares analysis.

Chapter 4

Experimental and Theoretical Results

In this chapter, the Raman spectra of several aqueous solutions are examined and briefly discussed. Raman spectra of aqueous halides and pseudohalides have been obtained over a number of years. Reviews of previous studies of water and aqueous solutions contain most of the essential background, for example, Tödheide (1972), Brooker (1986, 1988), Terpstra *et al.* (1990) and the IR work of Janoschek (1982). The principle goal of the present investigation was to establish the origin of the polarised component in the 150 to 300 cm^{-1} region of the isotropic spectrum of aqueous halides and pseudohalides.

In the theoretical section, *ab initio* calculations of several anion-water species are presented. The theoretical and experimental results are compared

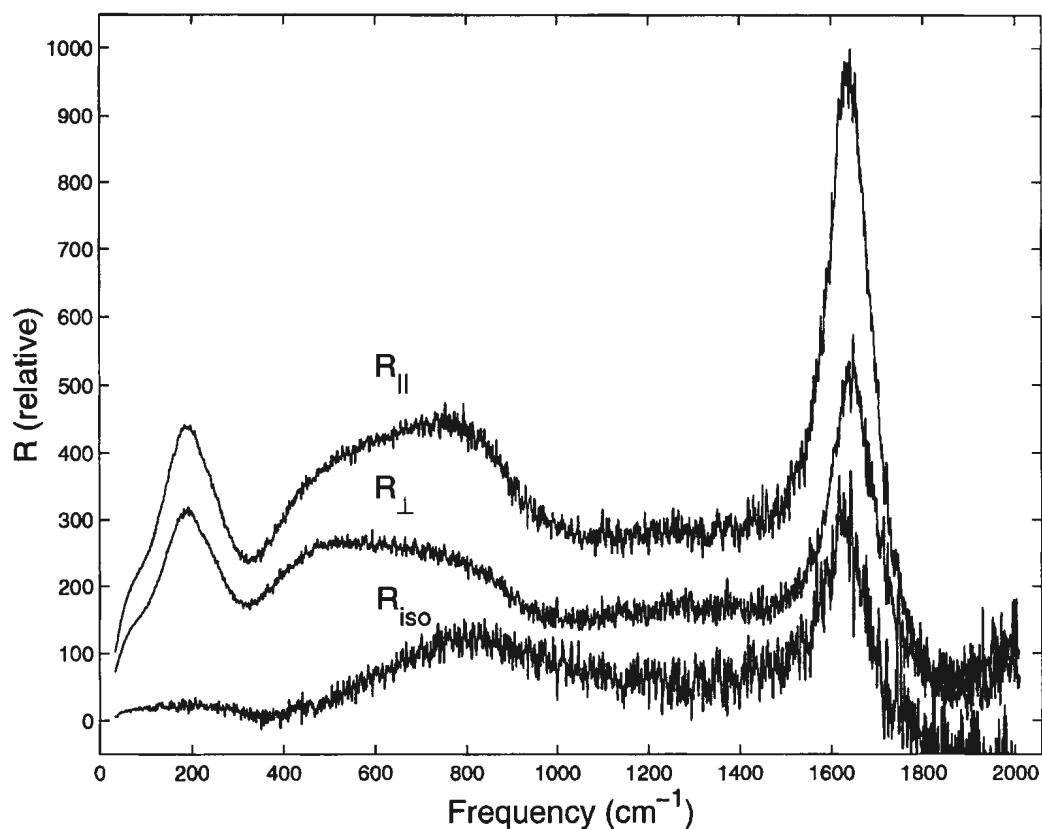


Figure 4.1: $R_{||}$, R_{\perp} and isotropic spectrum of pure water

and contrasted in Chapter 5.

4.1 Low Frequency Raman Spectra

4.1.1 Pure Water and Aqueous Halides

The low frequency Raman spectrum of pure water at 25 °C, Fig. 4.1 shows a number of bands below 2000 cm^{-1} . The $R_{||}$ curve is the normalised intensity of light scattered in the $[X(ZZ)Y]$ geometry which is polarised. The depo-

larised [X(ZX)Y)] intensity given by the R_{\perp} curve, arises from non-symmetric vibrational modes. The lower curve is the isotropic intensity, associated with the symmetric components of the polarisability tensor and is calculated from R_{\parallel} and R_{\perp} using Eqn. 2.24. Between 400 and 1200 cm^{-1} are several components that are likely due to librational modes between water molecules and small clusters. The similarity of the R_{\parallel} and R_{\perp} spectra indicate that most of the intensity is depolarised. However, there are weak isotropic bands between 190 and 800 cm^{-1} . Both bands have been observed throughout the study. Just above 1600 cm^{-1} is the ν_2 or bending mode of water. The isotropic intensity below the ν_2 peak is very low and consists of a broad band near 800 cm^{-1} . This may be due to a slightly polarised component of the wagging modes of water. A weak signal near 190 cm^{-1} has been assigned to the hydrogen bond stretch between pairs of water molecules or clusters (Brooker, 1986) and references cited therein. Other bands in the unpolarised spectrum below 200 cm^{-1} been resolved (Mizoguchi *et al.*, 1992).

As ammonium sulphate was used as an internal standard for these experiments, it was necessary to demonstrate that neither NH_4^+ or SO_4^{2-} contributed significant intensity in the 0 to 400 cm^{-1} region. Because NH_4^+ and SO_4^{2-} are spherically symmetric, there will be very little intensity associated with

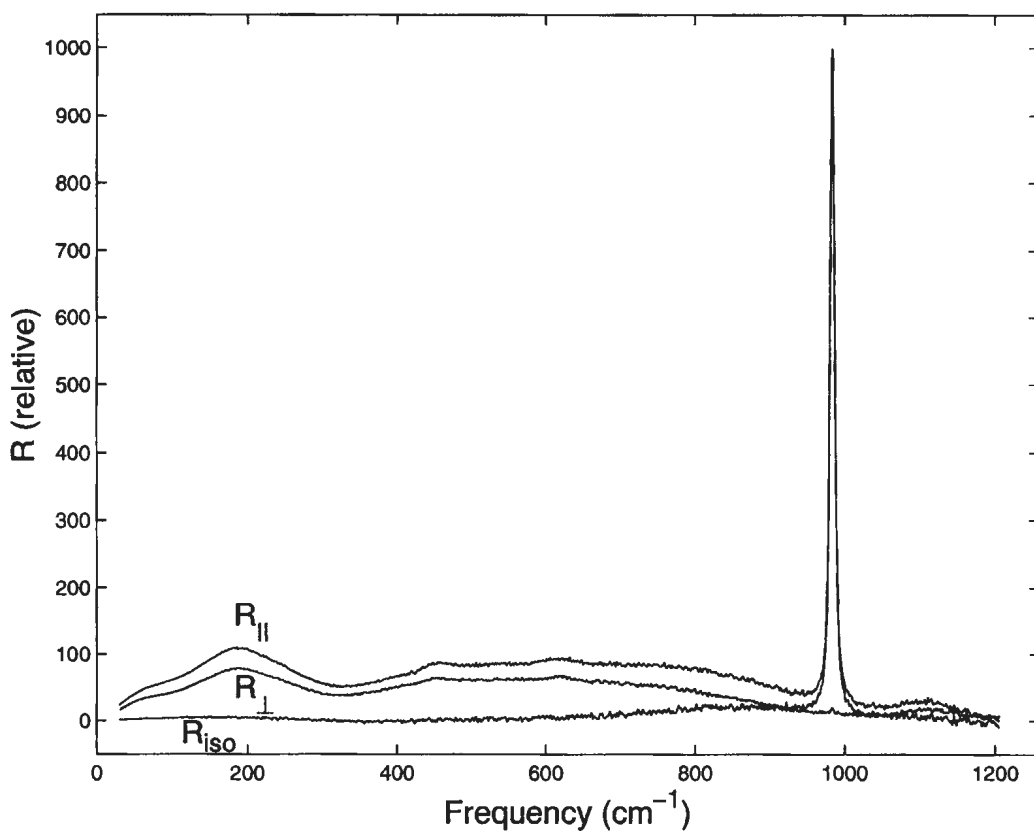


Figure 4.2: $R_{||}$, R_{\perp} and R_{iso} aqueous 0.1 molar $(\text{NH}_4)_2\text{SO}_4$

reorientational motions in this region. This was confirmed by studies of a solution of $0.1 \text{ mol}\cdot\text{L}^{-1}$ ammonium sulphate, Fig. 4.2. The intense ν_1 peak of sulphate is at 980 cm^{-1} . Weak depolarised components due to ν_2 and ν_4 activity can be detected near 460 and 630 cm^{-1} in the $R_{||}$ and R_{\perp} but are not present in the R_{iso} spectrum. Isotropic activity below 600 cm^{-1} is very low confirming that the baseline subtraction calculation is valid. The $R_{||} - \frac{4}{3}R_{\perp}$

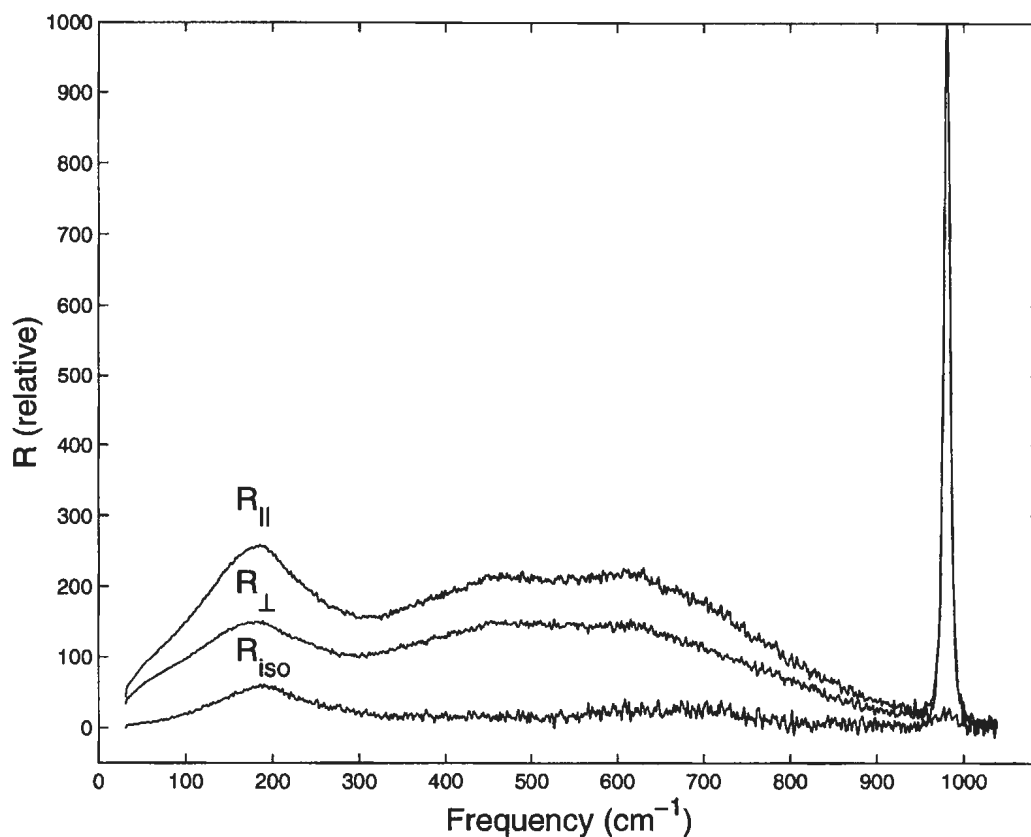


Figure 4.3: $R_{||}$, R_{\perp} and R_{iso} of 5 molar NH_4Cl

difference is close to zero as would be expected for the asymmetric modes but as was the case for pure water, there is weak intensity at about 190 and 800 cm^{-1} . In addition, it is confirmed that sulphate and its counter ion, ammonium, do not appreciably interfere with the low frequency isotropic region. Ammonium sulphate is therefore satisfactory as an internal standard and ammonium is an appropriate counter-ion in aqueous halide studies.

Similar results were obtained with K_2SO_4 and $NaClO_4$ as internal standards. The residual isotropic activity in the 500-800 cm^{-1} region may be associated with symmetric wagging modes between water pairs and transient clusters of water molecules.

A 5.0 molar solution of ammonium chloride showed a significantly more intense isotropic peak at 185 cm^{-1} than water, Fig. 4.3, lower trace. The top and middle traces correspond to the intensities in the parallel and perpendicular scattering geometries, respectively.

To determine the dependence of the low frequency band of the anion, spectra for 5.0 molar ammonium salts of fluoride, chloride, bromide and iodide were scanned from 30 to 1200 cm^{-1} with 0.1 $mol \cdot L^{-1}$ sulphate as the internal standard. Isotropic intensities were calculated and scaled such that the internal standard peak was of equal intensity for each spectrum. All scans were then superimposed, Fig. 4.4, and the peaks identified according to the anion, Fig. 4.5.

Two distinct trends in the low frequency spectra of the halides were exhibited as the atomic number of the halide is increased. First, the intensity of the corresponding peak increased and second, the frequency of peak maximum decreased. Spectra of haloacids and halide salts of other cations were

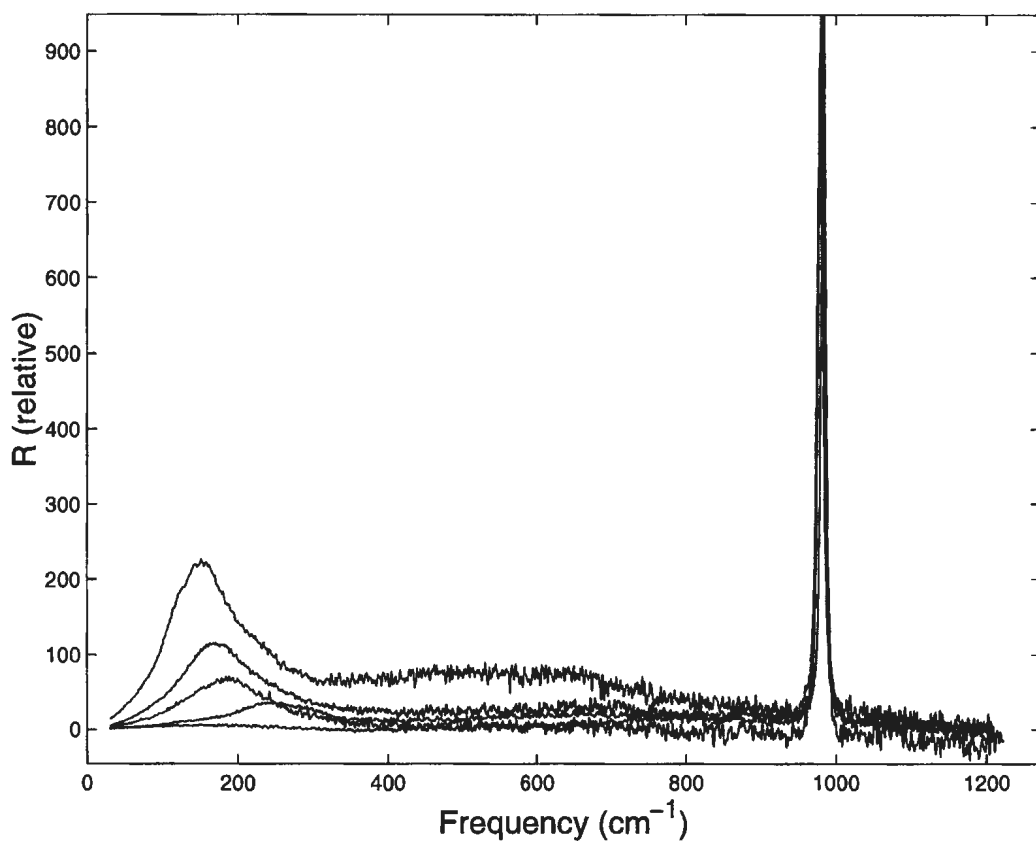


Figure 4.4: Isotropic spectra of 5 molar $\text{NH}_4\text{-I}$, Br , Cl , F and H_2O

shown to produce the same trends (Brooker, 1996) and so these bands are essentially cation independent. The peak for concentrated acids were observed a few wavenumbers higher than those for the ammonium salts, however. It is also apparent that the symmetric shape of the bands diminishes along the halide series.

The increase in the isotropic intensity for the iodide spectrum in the 300-

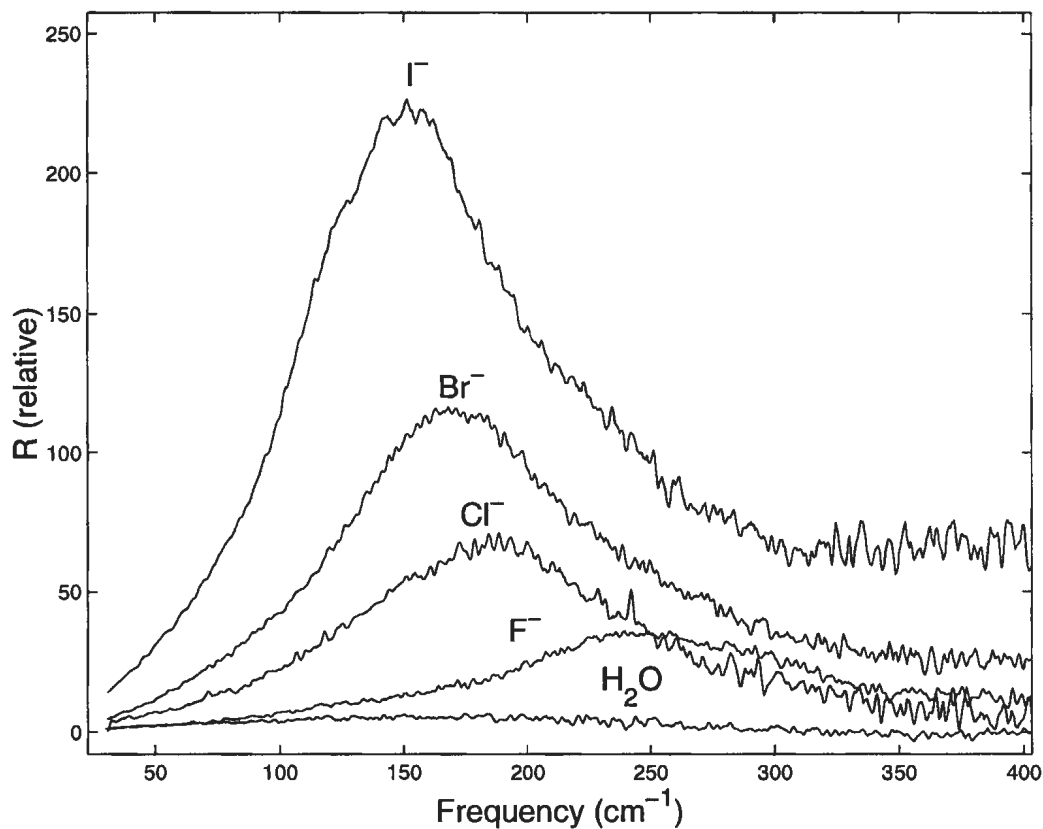


Figure 4.5: Expanded spectra of Fig. 4.4

800 cm^{-1} region is notable in Fig. 4.4. This feature may originate from librational modes induced by the presence of iodide ions.

4.1.2 Other Anions

Polarised low frequency bands were also observed for other anions. Sodium hydroxide and cyanide solutions exhibited bands in the isotropic spectrum similar to those for the halides. For 5 molar NaOH, Fig. 4.6, the peak was

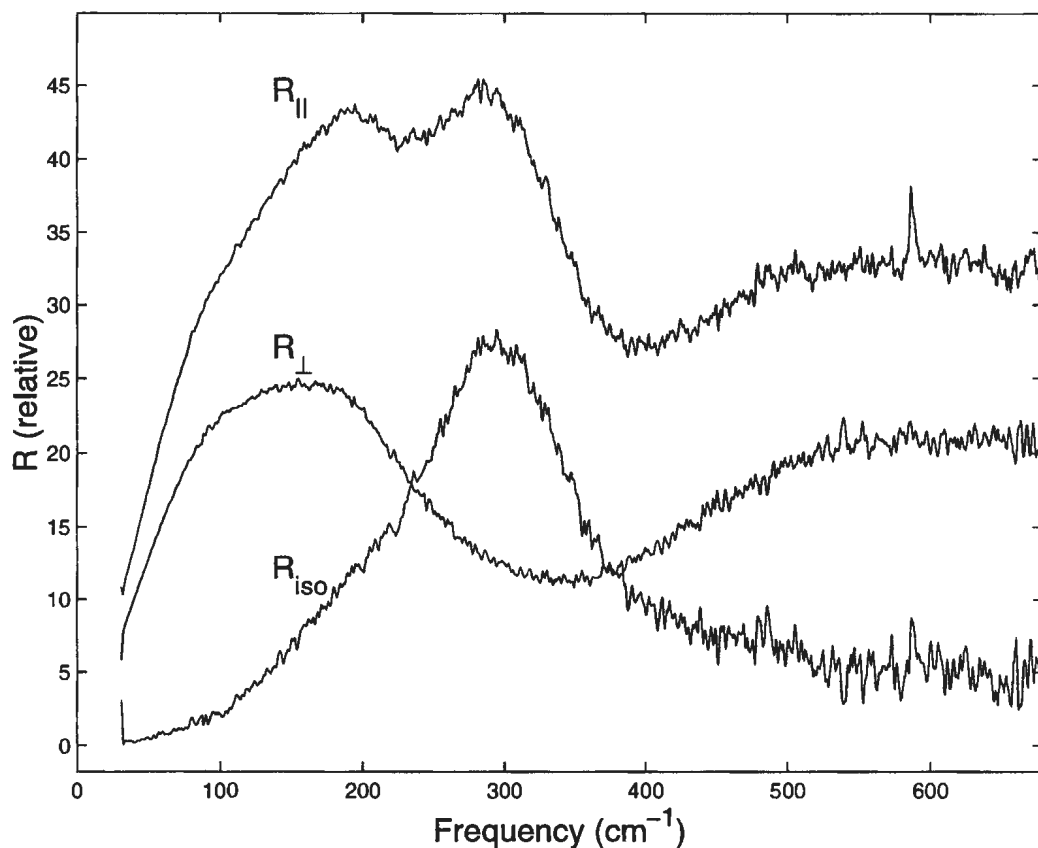


Figure 4.6: $R_{||}$, R_{\perp} and R_{iso} of 5 molar NaOH in H_2O

near 290 cm^{-1} while for five molal NaCN, Fig. 4.7, it was 200 cm^{-1} . The librational modes of the cyanide ion in solution contributed significantly to the depolarised intensity in the low frequency region at about 130 cm^{-1} , but the isotropic peak is clearly defined in the spectrum at a higher frequency of 200 cm^{-1} . The cyanide ion is not spherically symmetric and therefore has intensity at 130 cm^{-1} due to reorientational motion of the cyanide ion

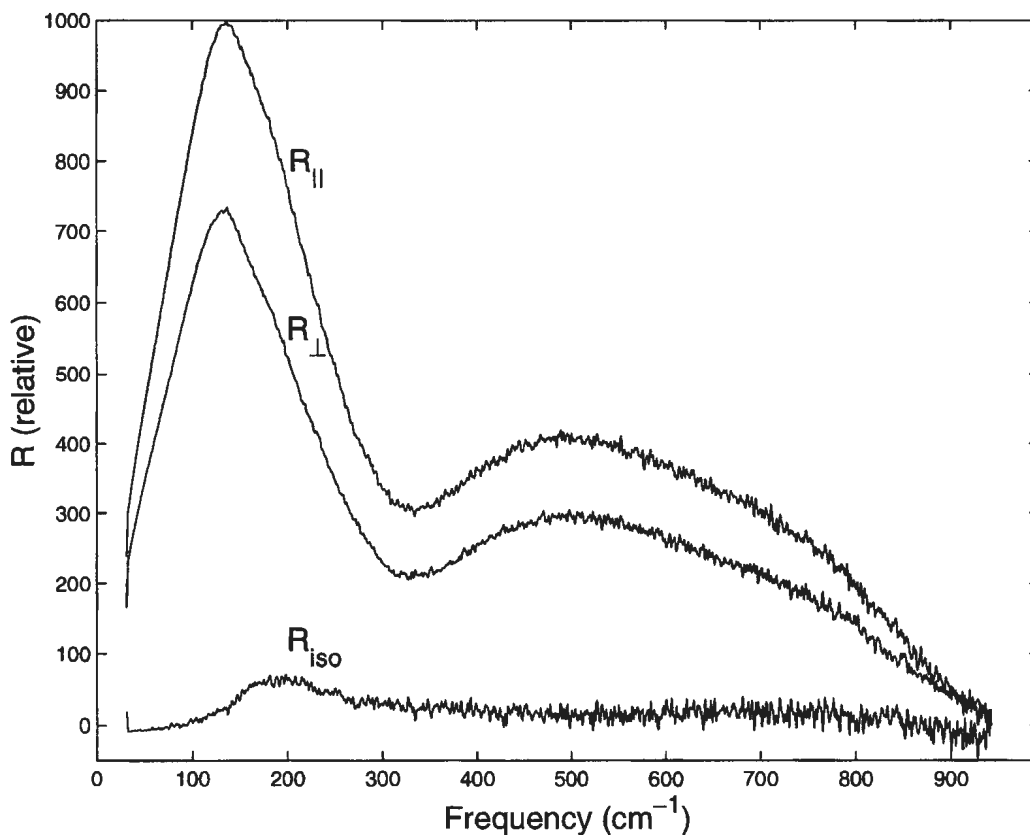


Figure 4.7: $R_{||}$, R_{\perp} and R_{iso} of 5 molal NaCN in H_2O

superimposed on the depolarised intensity of water.

4.1.3 Isotope Substitution Studies

Isotope effects were investigated by examining spectra of 5 molar solutions of ND_4Cl , $NaOD$ in D_2O and $Na^{18}OH$ in $H_2^{18}O$. The spectrum of ND_4Cl was scanned to 4000 cm^{-1} to verify that there was no contamination by 1H_2O whose ν_1 and ν_3 peaks would appear around 3700 cm^{-1} . The spectrum of

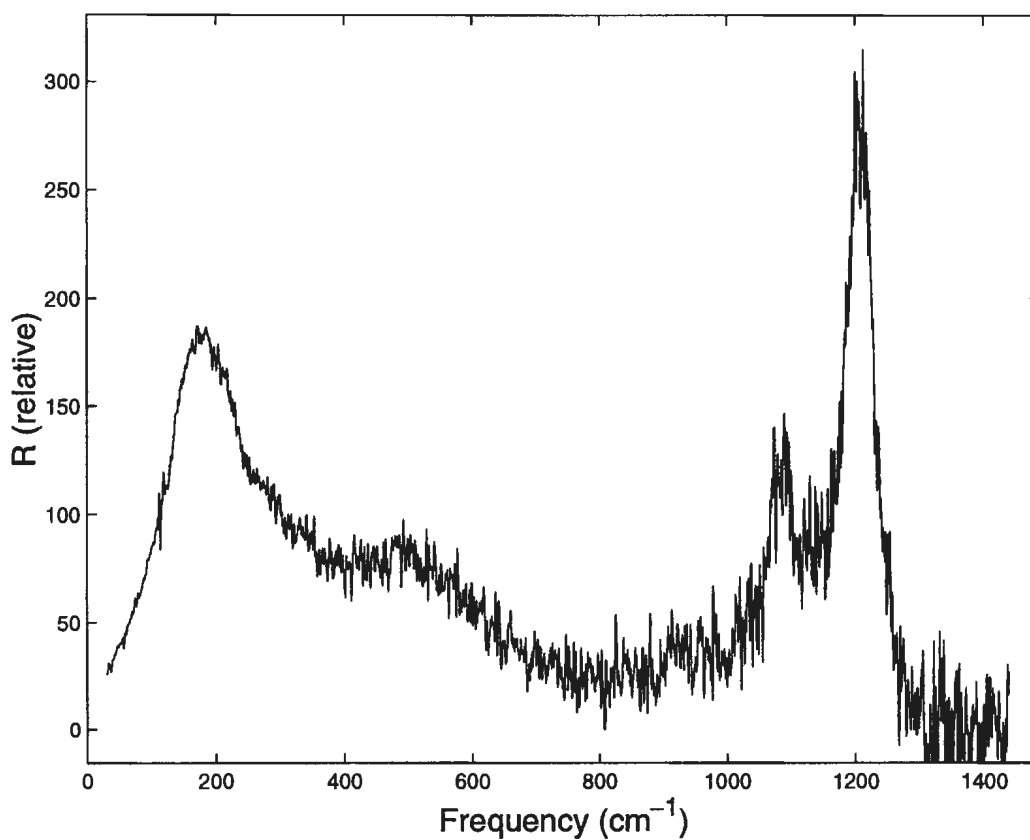


Figure 4.8: Isotropic spectrum of 5 molar ND_4Cl in D_2O

ND_4Cl (Fig. 4.8) shows the ν_2 mode for ND_4^+ and the ν_2 mode of D_2O at 1100 and 1200 cm^{-1} respectively. There is some interference from the residual wagging motions of D_2O in the 300-600 cm^{-1} region. Fig. 4.9 shows the low frequency peak to be slightly lower in frequency than the corresponding peak for NH_4Cl .

Fig. 4.10 shows spectra of NaOH in H_2O with the ^{16}O and ^{18}O isotopes.

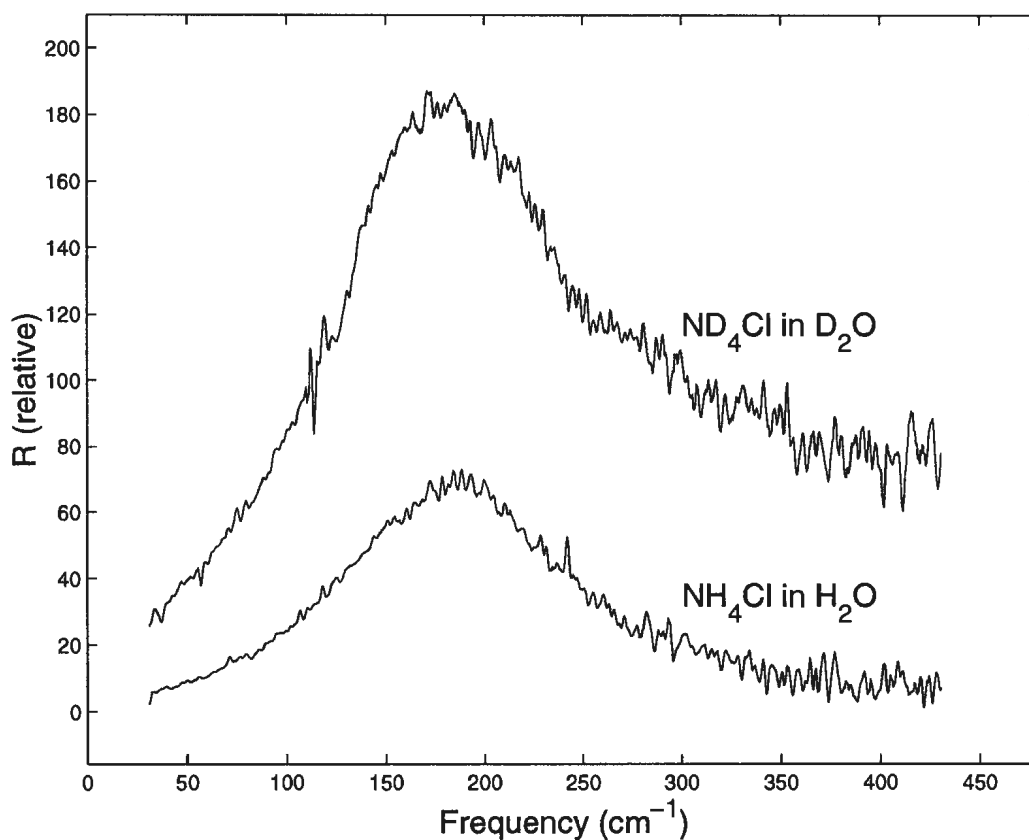


Figure 4.9: Isotropic spectra of 5 molar ND_4Cl in D_2O and NH_4Cl in H_2O

A red shift for the 290 cm^{-1} band is evident for the heavier isotope. Because of the small sample size, only the polarised component could be measured but the second polarised peak is at the same frequency relative to the maximum in the isotropic spectrum, Fig. 4.6. A red shift was also observed for OD^- in D_2O relative to OH^- in H_2O .

Work by Kameda *et al.* (1994) on aqueous lithium bromide has shown

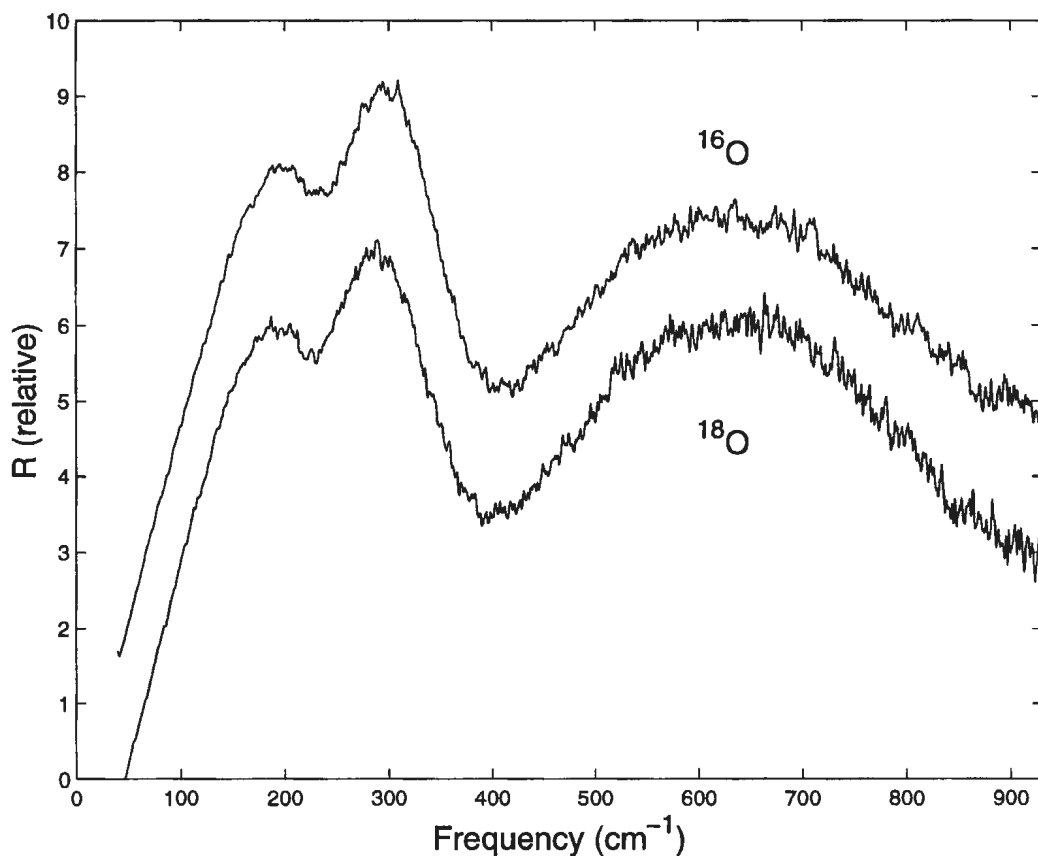


Figure 4.10: $R_{||}$ for NaOH in H_2O and with ^{18}O substitution

that the low frequency peak was red shifted by about 10 cm^{-1} in D_2O solutions.

The low frequency isotropic peak of concentrated DBr in D_2O was actually found to be slightly higher than that for NH_4Br in H_2O , but these solutions are not directly comparable. The differences in the cations and the concentration may have contributed to the blue shift.

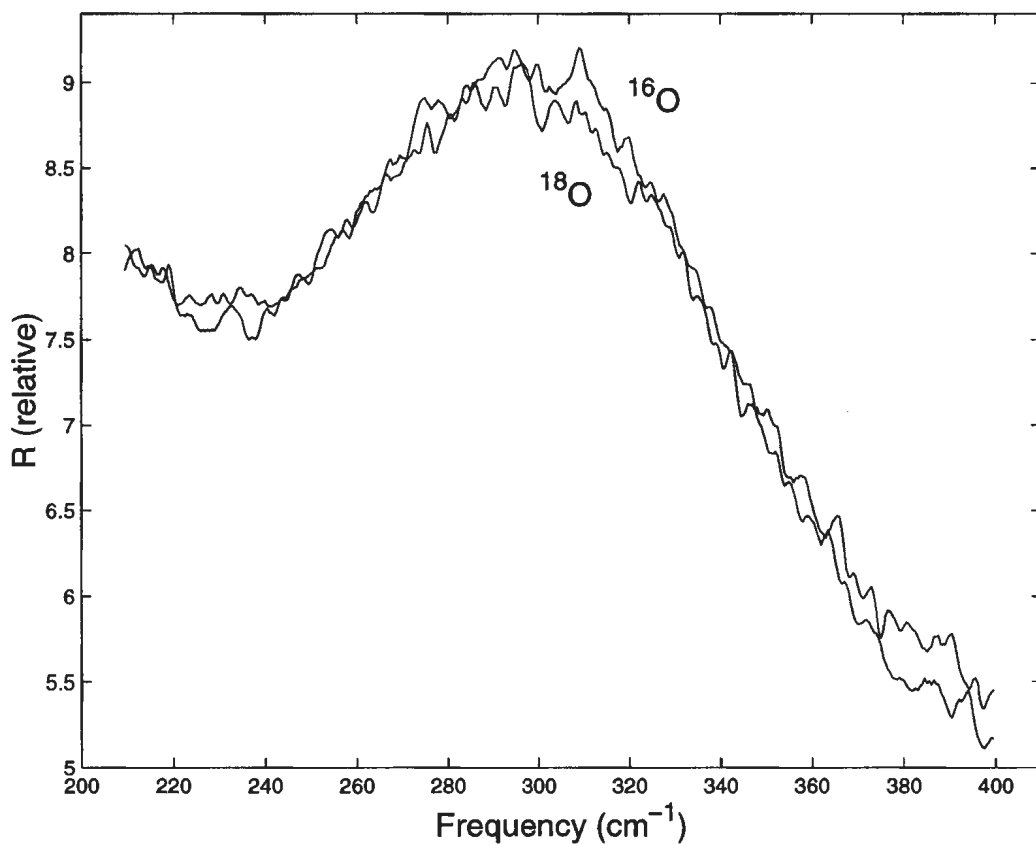


Figure 4.11: $R_{||}$ for NaOH in H_2O : ^{18}O curve shifted $+7\text{ cm}^{-1}$

4.1.4 The Influence of Temperature

The low frequency peak persisted as the temperature of the sample was increased. Spectra of 5.0 molar solutions of NH_4Cl and NaOH with sulphate and nitrate respectively as internal standards were taken at higher temperatures. Isotropic spectra for both solutions were obtained at three temperatures, Fig. 4.12 and Fig. 4.13.

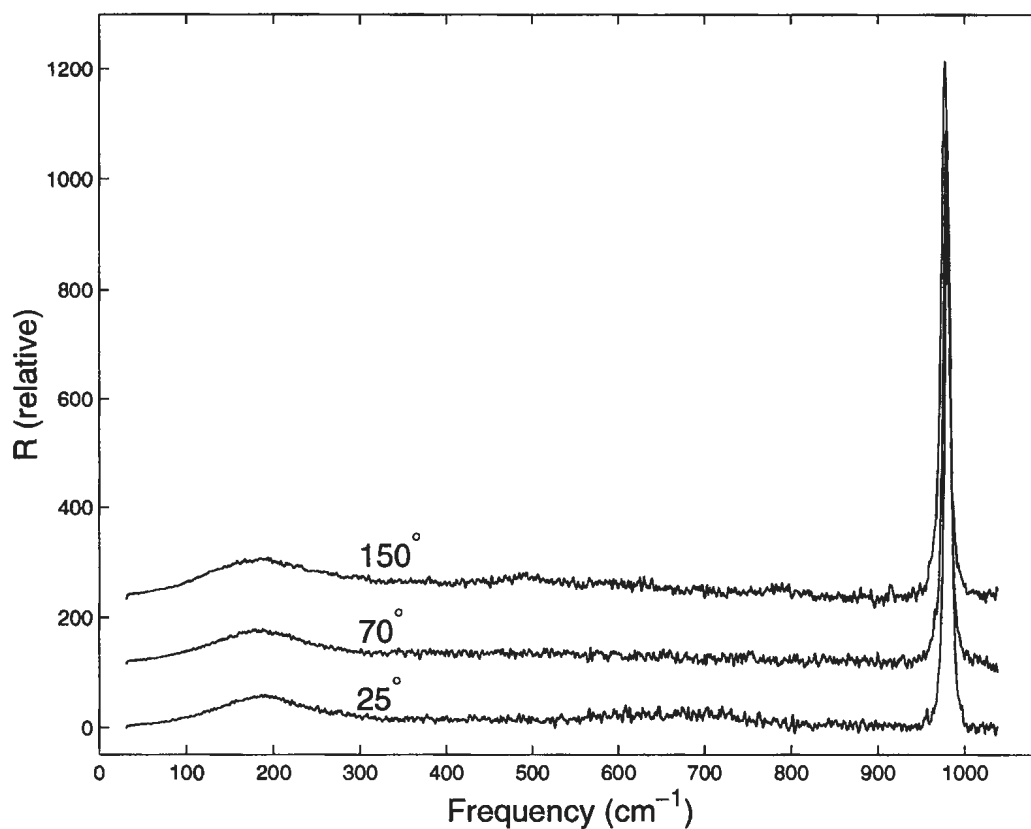


Figure 4.12: Isotropic spectra of NH_4Cl in H_2O at 25, 70 and 150 °C .

As the temperature was increased, all peaks, including those of the internal standards appeared to decrease very slightly. There was a marked increase in the width of the peaks with increasing temperature. It is clear that the species responsible for the low frequency polarised band can exist at temperatures well above the normal boiling point of water. Two new peaks appeared at 760 and 930 cm^{-1} in the hydroxide spectrum at 130 °C, Fig.

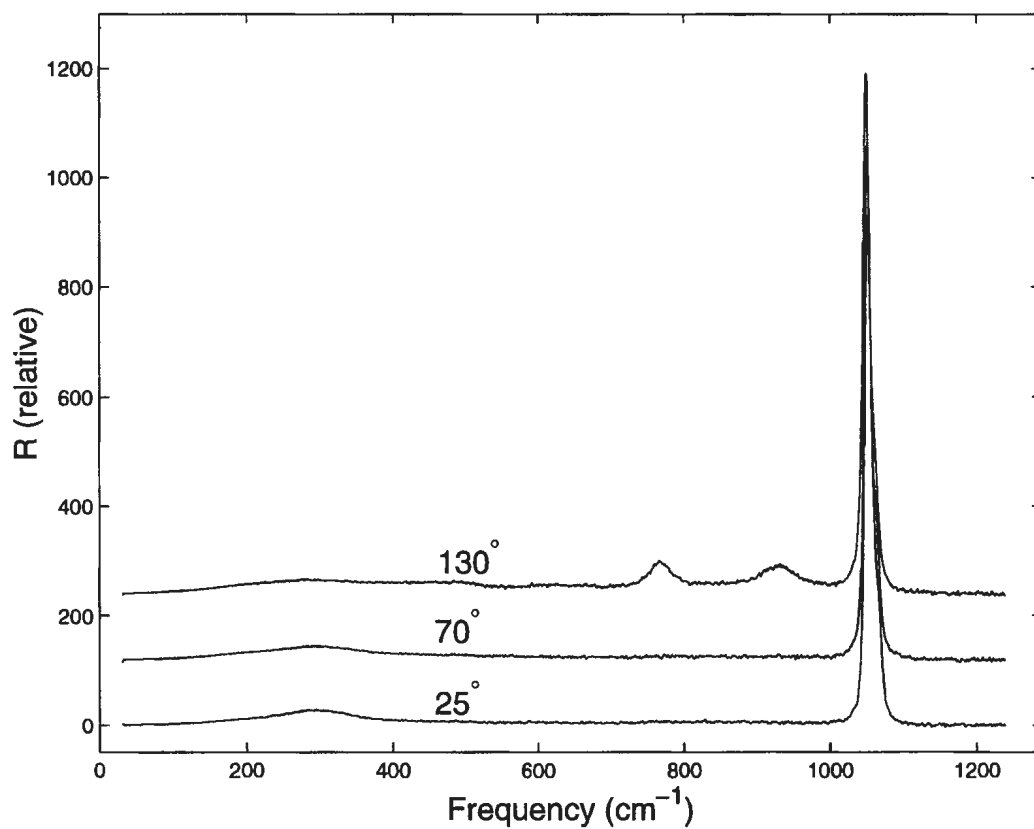


Figure 4.13: Isotropic spectra of NaOH in H₂O at 25, 60 and 130 °C

4.13. These were present in the spectrum after the sample was cooled to room temperature and are likely due to hydroxides of silicon such as $\text{SiO}_2(\text{OH})_2^{2-}$ (Freund, 1973). This is consistent with the etching of the quartz cuvette observed after the experiment.

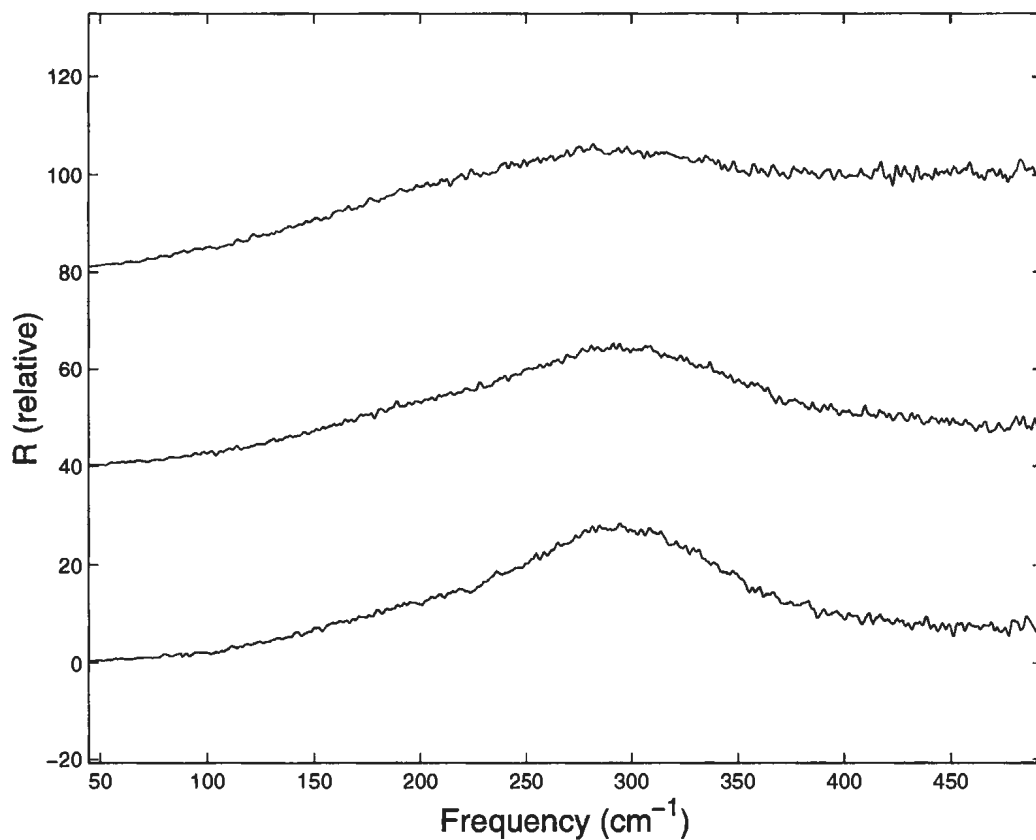


Figure 4.14: Expanded spectra of NaOH in H₂O at 25, 60 and 130 °C

4.1.5 Evaluation of Spectroscopic Parameters

Band position centre frequencies, ν , intensities, R , and full widths at half heights, Γ were determined for all isotropic spectra that were taken. In each instance, a Gaussian curve was used over the range corresponding to the upper half of the peak. Attempts to curve fit larger regions resulted in the fitted curve having a poor fit and a higher centre frequency than the

experimental peak. It is clear that the peaks are not pure Gaussian and appear to have high frequency shoulders, particularly as the atomic number increased. Hydrogen bond stretching bands have been shown by Marechal and Bratos (1978) to have an asymmetrically distorted Gaussian shape. It is therefore necessary to use the upper half of the peak for curve fitting because this distortion cannot be accommodated by pure Gaussian model curves. In addition, the broad and weak 800 cm^{-1} band may overlap the high frequency side of these peaks and further increase the distortion. The uncertainty in the centre frequency by this method was approximately $\pm 3\text{ cm}^{-1}$. Because the low frequency bands are relatively weak it was difficult to obtain consistent integrated intensities for the peaks. The intensities were therefore taken to be the relative heights on the R axis with the 0.1 M sulphate internal standard having an intensity of 1000. The intensities of the cyanide and hydroxide cannot be directly compared with the others because the cyanide spectrum was taken without an internal standard and nitrate was used as the internal standard in the hydroxide study. The results are tabulated in Table 4.1.

Isotopic red shifts were evaluated by translating the isotopically substituted spectra to higher wave numbers until the RMS difference between the intensities of the substituted and non-substituted spectra reached a mini-

Table 4.1: Spectroscopic parameters for the low frequency bands of aqueous halides

Associated Anion	ν (cm^{-1})	R	Γ (cm^{-1})
(Water)	190	5	268
Fluoride	252	34	147
Chloride	185	65	130
Bromide	173	113	121
Iodide	151	219	110
Cyanide	200	.	252
Hydroxide	293	.	147

num value. The range over which the RMS difference was evaluated was the peak width at half height. The red shift was taken as the translation at this point, Fig. 4.11 for example, and recorded in Table 4.2. This was found to give a more dependable value for the shift than could be obtained from the difference in the centre frequencies as determined by curve fitting.

Table 4.2: Isotopic red shifts

Anion/Isotope	Red shift (cm^{-1})
$\text{OD}^-/\text{D}_2\text{O}$	7
$^{18}\text{OH}^-/\text{H}_2^{18}\text{O}$	22
$\text{Cl}^-/\text{D}_2\text{O}$	4

Similar intensity scaling and curve fitting procedures were used to determine the effects of increased temperature on the spectra for chloride and hydroxide. The results are tabulated in Tables 4.3 and 4.4 respectively.

Table 4.3: Effect of temperature on the low frequency chloride band

T (°C)	ν (cm ⁻¹)	R	Γ (cm ⁻¹)
25	189	56	133
70	188	54	137
150	186	64	159

Table 4.4: Effect of temperature on the low frequency hydroxide band

T (°C)	ν (cm ⁻¹)	R	Γ (cm ⁻¹)
25	295	27	147
60	293	25	187
130	292	24	252

4.2 Theoretical Results

4.2.1 *Ab Initio* Molecular Geometries and Energies

Much of the preliminary computational work was done using MUNGAUSS (Poirier *et al.*, 1995) on an SGI Indigo 2 workstation. Optimised geometries, molecular energies and harmonic frequencies at the RHF/6-31+G* level for F⁻(H₂O)_n were obtained for $n = 1 - 10$. Larger basis sets and second derivative calculations required for force constant determinations were not then implemented by MUNGAUSS hence further calculations were performed using Gaussian92 and Gaussian94 (Frisch *et al.*, 1995) on a DEC AlphaServer 4100 symmetric multiprocessor computer. Basis sets for iodine were unavail-

Table 4.5: Optimised structures for water and the anion hydrates

X	$R_1(\text{\AA})$	R_2	R_3	R_{OX}	α ($^\circ$)	β
(H ₂ O)	.	0.9412	0.9412	.	.	106.2208
OH	1.5815	1.0026	0.9398	2.5775	171.5684	102.6328
F	1.5142	0.9959	0.9395	2.5046	172.2750	102.9450
CN	1.9632	0.9597	0.9403	2.9006	164.9073	102.9389
Cl	2.3950	0.9546	0.9408	3.2930	156.6069	102.2432
Br	2.6445	0.9514	0.9412	3.5132	152.0231	102.3404

able. The optimisation scheme used by MUNGAUSS was more efficient and less likely to terminate unnecessarily.

Except as indicated, all results were obtained using the 6-311++G** basis sets. Geometries and energies were obtained at the spin restricted Hartree-Fock and post Hartree-Fock level for the anion monohydrates. Very tight convergence criteria were used in anticipation of the broad potential minimum that is expected about a hydrogen bond. This ensured that an accurate minimum energy geometry was used for calculating the second derivatives of the energy and the molecular force constants (Hehre *et al.*, 1986). Use of normal convergence criteria lead to subtle errors in the energy and differences in the vibrational frequencies of several wavenumbers.

The results for the anion monohydrates are presented Table 4.5 and are listed in order of increasing reduced mass. The geometric parameters are designated according to Fig. 4.15. Although it is instructive to consider the

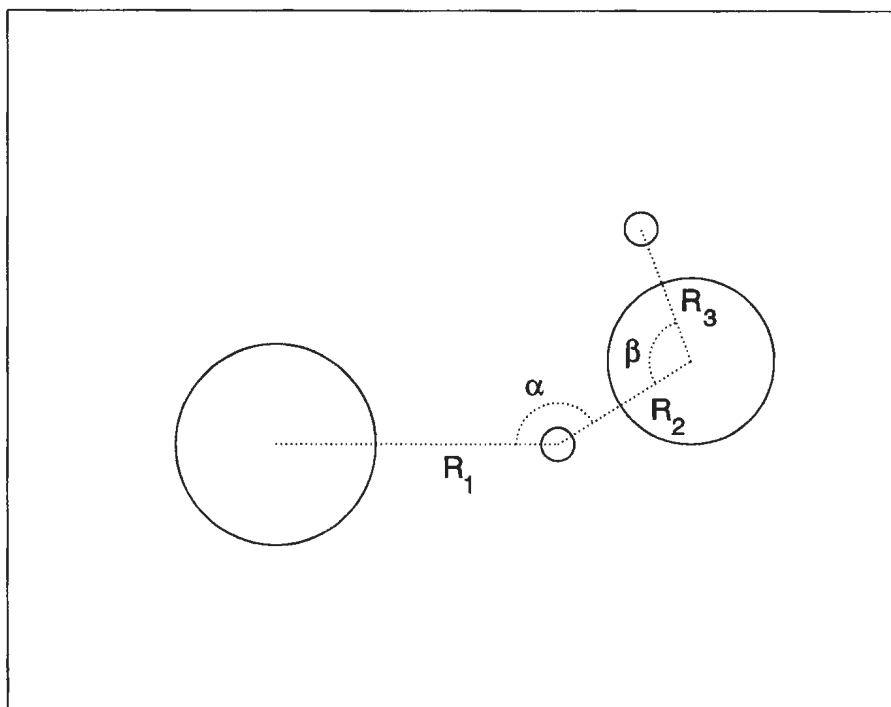


Figure 4.15: Parameters of the molecular geometry

hydrogen bond length, R_1 as a parameter, the oxygen-anion distance R_{Ox} is preferred because it eliminates the ambiguity of the two hydrogen-anion distances in the complex. In addition, much of the x-ray diffraction data in the literature uses this measurement. These geometries correspond to the minimum energy configuration on the potential hypersurface. Optimisations to transition state geometries were precluded by performing a supplemental normal mode frequency calculation. Any geometry that yielded one or more

normal modes with an imaginary frequency was discarded.

Sharpe (1990) cited two limiting structures for anion monohydrates: a linear hydrogen bond to only one hydrogen and bidentate bonding to both hydrogens of the water molecule. The calculated structure for all monohydrates was between these two structures, i.e., the anion bonded to only one hydrogen and formed an XHO angle of less than 180° . Interestingly, the hydroxide was the only species that was not flat. The hydroxyl proton was consistently out of the plane formed by the rest of the complex at all levels of calculation. Constraining the complex to be coplanar increased the energy by 0.48 kJ mol^{-1} . For hydroxide, the OO distance was 2.577 and the O-hydroxyl H distance was 3.144 Å. Cyanide had an OC and ON bond distances of 2.901 and 4.040 Å respectively.

Several trends were apparent in the molecular geometry along the series of halide hydrates. As the atomic number increased, the hydrogen bond length increased and the included angle, XHO decreased. In addition, the effect of the anion in perturbing the geometry of the hydrating water decreased along the series. The effect on the HOH bond angle was not as strong as that on the differential stretching of the OH bonds. For the fluoride species, the free OH bond length was significantly shortened whereas the OH distances of

bromide hydrate were essentially equal. The perturbation of the H-bonded OH bond length was about 5 percent greater for fluoride than for chloride but was negligible for bromide hydrate. A more pronounced difference was observed in the MP2 results.

To test the *ab initio* calculations for convergence, the chloride hydrate complex was optimised with several basis sets and levels of theory (Table 4.6.) Convergence of geometry with the basis set was evident at the RHF level because a small (0.6 percent) decrease in the hydrogen bond distance resulted as the basis set was made larger. The energy decreased as would be expected from a variational method, but less quickly. More pronounced effects were apparent for the calculated charge of the chlorine atom and the frequency of the lowest energy vibrational mode. At the Møller-Plesset levels, the hydrogen bond length fluctuated about a value of 2.16 Å and the frequency decreased slightly. More significant was the difference between the RHF and CISD results. The lower energy of the latter suggests that electron correlation is a significant factor.

These results are all reasonably close, but the presence of what appears to be a small dependence on the level of theory and basis set size suggests that more advanced calculations may be warranted to confirm that convergence

Table 4.6: Convergence of parameters by basis set and theory level for chloride monohydrate

Theory/Basis Set	$R_{XH}(\text{\AA})$	E(Hartrees)	Cl At. Charge	ν (cm^{-1})
RHF/6-31+G*	2.409759	-535.5774642	-0.974718	153.7036
RHF/6-31++G**	2.397843	-535.5907395	-0.960972	152.5437
RHF/6-311++G**	2.395022	-535.6384496	-0.949027	148.2248
MP2/6-311++G**	2.150397	-536.0032515	-0.924436	184.5516
MP3/6-311++G**	2.184821	-536.0159339	-0.928804	178.6977
MP4/6-311++G**	2.158792	-536.0300185	-0.925195	.
CISD/6-311++G**	2.215327	-535.9884134	-0.932160	173.4514

has been reached. It is clear that the results are *near* convergence and any error is likely to be systematic so that valid comparisons may be made on the relative properties of the different complexes.

4.2.2 Normal Mode Force Constants and Frequencies

Harmonic force constants of the normal modes were calculated by the Gaussian packages using the harmonic approximation and group theory. In addition, simulation data were calculated so that the normal mode vibrations could be animated and the dynamics of the vibrations could be seen. For all the halide complexes, hydrogen bond stretching occurred only in the lowest frequency mode. This mode was essentially a pure hydrogen bond stretch in the animation with only traces of other components such as slight changes in the adjacent OH bond length and the orientation of the water molecule

Table 4.7: Experimental and theoretical frequencies (cm^{-1})

X	Expt	RHF	MP2	MP3	CISD	DFT
F	252	309	371	369	356	368
Cl	185	148	185	178	180	184
Br	173	118	145	140	136	129
OH	293	282	280	280	296	.
CN	200	196	218	218	211	.

whose atoms moved coherently during the vibration. Hydrogen bond stretching was observed in the third mode for cyanide hydrate, and was dominant in the second but distributed over several low frequency modes for hydroxide hydrate.

The frequencies for these modes at several levels of theory are given in Table 4.7 along with the corresponding centre frequency of the low frequency Raman band. The available Gaussian documentation was unclear as to the validity of the MP3 frequencies. The DFT results were obtained at the BLYP level, (Lee *et al.*, 1988) but convergence could not be achieved with the hydroxide and cyanide complexes.

The effect of isotope substitution was determined by using the *ab initio* force constants for the most abundant isotope and recalculating the normal mode frequency with the desired isotopic mass. Using previously calculated

force constants, frequencies for the hydrogen bond stretch were calculated for deuterium and ^{18}O isotopomers.

The calculated and experimental low frequencies for anion complexes and isotopomers are tabulated in Table 4.8 along with the inverse square root of the reduced mass of each complex in AMU calculated as $[(m_X^{-1} + m_{\text{H}_2\text{O}}^{-1})^{-1}]^{-\frac{1}{2}}$. This quantity was useful in scaling isotope frequencies in accordance with the harmonic oscillator model. Experimental isotope frequencies were tabulated as the normal isotopomer frequency minus the isotope shift, to preserve the consistency of the shift as determined by the spectrum shift and minimum difference method. The calculations for chloride hydrate apply to ^{35}Cl . For ^{37}Cl , the RHF frequencies in H_2O and D_2O were 147 and 143 cm^{-1} respectively. The last column in this table is the RHF binding energy in kJ mol^{-1} , calculated as $E_{\text{XH}_2\text{O}} - E_X - E_{\text{H}_2\text{O}}$.

In principle, it should be possible to determine the energy distribution of the motions comprising a normal mode and to quantify how much of the normal mode is a hydrogen bond stretch. It was unclear how to do this with the data from the Gaussian 94 calculations. Instead, isotope shifts were calculated using Eqn. 2.4. By inspection, it is clear that for a given force constant, the frequency will decrease by an amount equal to the square root

Table 4.8: Experimental and theoretical frequencies in H₂O and D₂O

Anion	$\mu^{-1/2}$	Expt	RHF	MP2	E_b
OH ⁻ /H ₂ O	0.3381376	293	282	280	101.85
OD ⁻ / D ₂ O	0.3247615	271	232	225	101.85
¹⁸ OH ⁻ /H ₂ ¹⁸ O	0.3202736	286	270	271	101.85
F ⁻ /H ₂ O	0.3288753	252	309	371	101.89
F ⁻ /D ₂ O	0.3202785	.	300	358	101.89
CN ⁻ /H ₂ O	0.3065615	200	196	218	58.74
CN ⁻ /D ₂ O	0.2973202	.	191	212	58.74
Cl ⁻ /H ₂ O	0.2900342	185	148	185	51.46
Cl ⁻ /D ₂ O	0.2802484	181	143	178	51.46
Br ⁻ /H ₂ O	0.2611403	173	118	145	44.21
Br ⁻ /D ₂ O	0.2502271	.	112	138	44.21

of the ratio of the reduced masses if the reduced mass is increased. Isotope frequencies calculated in this manner were found to be within one percent of the MP2 isotope frequencies for all anion hydrates but hydroxide. This confirms that the normal mode can be accurately modelled by the linear harmonic oscillator as a hydrogen bond stretch for the remaining anions.

Intensities were calculated from derivatives of the polarisabilities with respect to the electric field and were not satisfactory in reproducing the experimental results. For instance, the calculated intensities decreased with atomic number whereas the experimental intensities increased. Discrepancies were also noted in calculated Raman intensities on simple molecules: the F₂ and Cl₂ values were 23.8 and 46.5 Å⁴/AMU respectively, a ratio of 1:2.

Experimentally the ratio is 1:7 (Schrötter and Klöckner, 1979). Calculated Raman intensities can be unreliable (Frisch *et al.*, 1986).

4.2.3 Potential Energy Studies

Molecular interaction potentials have been studied for a number of systems, for example, by Ratajczak and Orville-Thomas (1980) and Gresh *et al.* (1975). *Ab initio* methods can provide much information about these potentials and their origin in terms of electrostatic forces, polarisation, dispersion and charge transfer mechanisms. Because the harmonic approximation is central to the calculation of frequencies, the nature of the potential about the hydrogen bond length was investigated to determine if it was indeed a harmonic potential. This was done by obtaining the optimised energy with the XO distance constrained to various values. Attempts to obtain potentials with respect to the XH distance yielded a spurious discontinuity in the potential associated with the two possible XH distances. This difficulty was precluded by using the former as a coordinate. The energy difference between potentials calculated about the two coordinates is small. The relative energies at the RHF, MP2 and CISD levels for the chloride hydrate complex are plotted along with the best-fit Morse potentials, Fig. 4.16. As the separation between the chloride ion and water molecule was further increased,

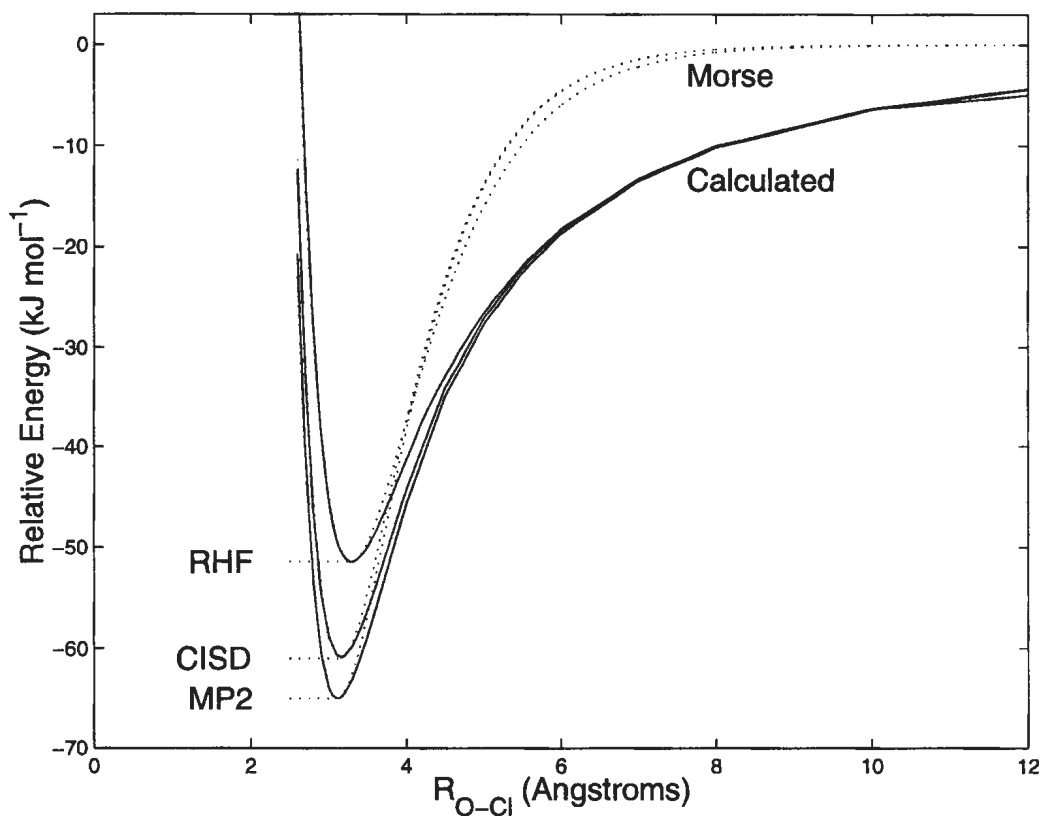


Figure 4.16: *Ab initio* and Morse potentials for $\text{Cl}^- \cdot \text{H}_2\text{O}$

the total energy increased monotonically and converged to a value equal to the sum of the energies for the chloride and water calculated independently. The reference potential energy in Fig. 4.16 was selected so that the zero energy level corresponded to the combined total energy of a noninteracting chloride ion and water molecule.

A comparison of the potential energy as a function of oxygen-anion dis-

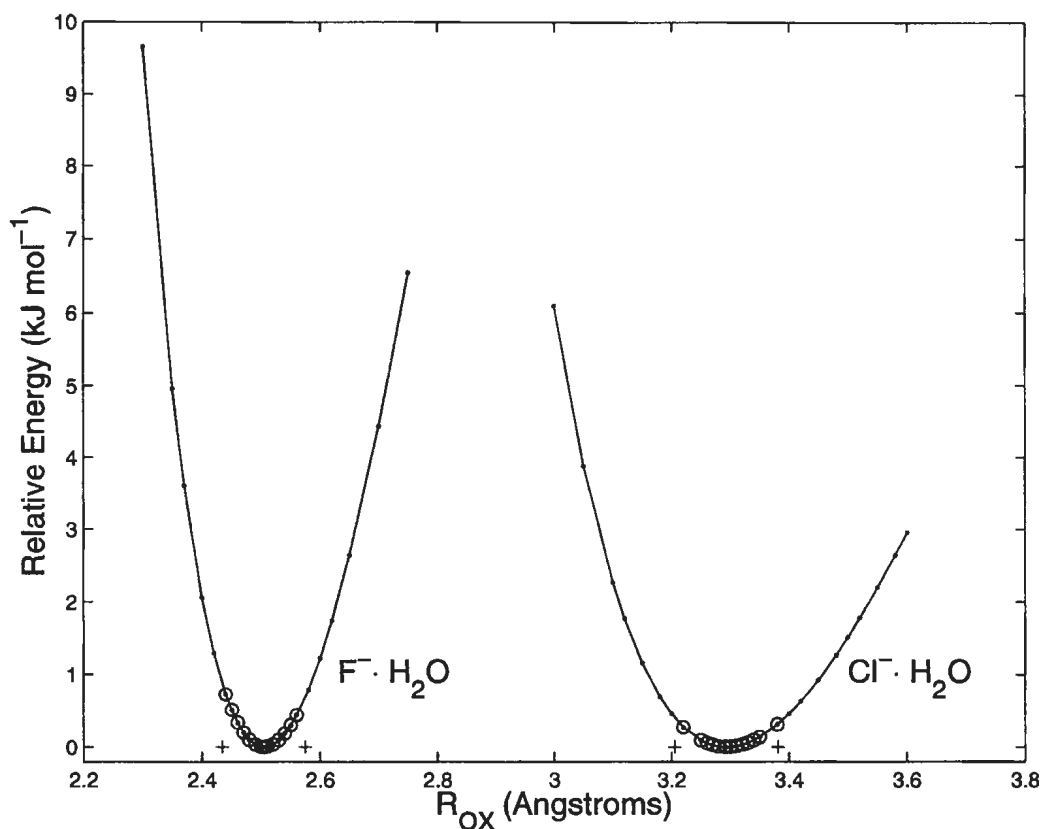


Figure 4.17: *Ab initio* potentials for $F^- \cdot H_2O$ and $Cl^- \cdot H_2O$

tance for fluoride and chloride ions in the vicinity of the equilibrium distance was obtained at the RHF level, Fig. 4.17. The crosses near the abscissa delineate the expectation value of the RMS amplitude and the circles a least square cubic fit to the calculated energy points over that range. This is further discussed in Chapter 5. The residuals of the cubic fit were of the order of 0.03 kJ mol^{-1} , an order of magnitude better than those for quadratic fit.

The curves were of very similar shape and could be superimposed by linear translation and scaling.

A similar energy section was calculated for hydroxide hydrate. The curve could be superimposed over the fluoride curve without scaling by translating it 0.1 Å to the left along the R_{OX} axis. No such data could be obtained for bromide hydrate. These calculations were based on a static system. The actual potential may be influenced by dynamic effects. For example, the molecule may not be in the minimum energy configuration with respect to the other degrees of freedom during the course of a vibration along the R_{OX} axis.

4.2.4 Multiple Hydration and Clusters

It is well known that cations can form discrete species with several water molecules (Brooker, 1986). The interaction is between a cation and the oxygen of the hydrating waters and the complex is relatively stable. Anion hydrates, on the other hand, depend on hydrogen bonds which are generally very short lived. Anion complexes with more than one water have been investigated theoretically by Kistenmacher *et al.* (1974), Xantheas *et al.* (1995) and experimentally in the gas phase by Arshadi and Kebarle (1970), who determined the high stability of the anion monohydrate. Payzant *et*

al. (1971) and Hiraoka and Mizuse (1988) have done experimental work on multiple hydration. Additional evidence such as X-ray diffraction (Beurskens and Jeffrey, 1964) has shown that such complexes exist in the solid state as octahedra of $F^-(H_2O)_6$ for potassium fluoride tetrahydrate. The hydrating waters were shared with the cations. The FO interatomic distances ranged from 2.71 to 2.78 Å in a structure comprising $K^+(H_2O)_6$ and $F^-(H_2O)_6$ octahedra.

Although spectroscopic evidence suggests that the anion is hydrogen bonded to only one water molecule on the picosecond time scale of the Raman measurement, an octahedral hydration sphere is possible in aqueous solutions. The anion would occupy an off centre position in the hydration cage, binding to one water molecule at any instant. Dielectric measurements of Holland and Lüty (1978) have provided evidence to suggest a similar model for cations in solid alkali halides.

It is energetically feasible for anion multihydrates to form, but the likelihood of their existence as formally hydrogen bonded systems must decrease as the level of hydration increases because aqueous hydrogen bonds have a lifetime on the order of picoseconds (Sharpe, 1990; Luzar and Chandler 1996), hence the probability of bonded multihydrates existing long enough

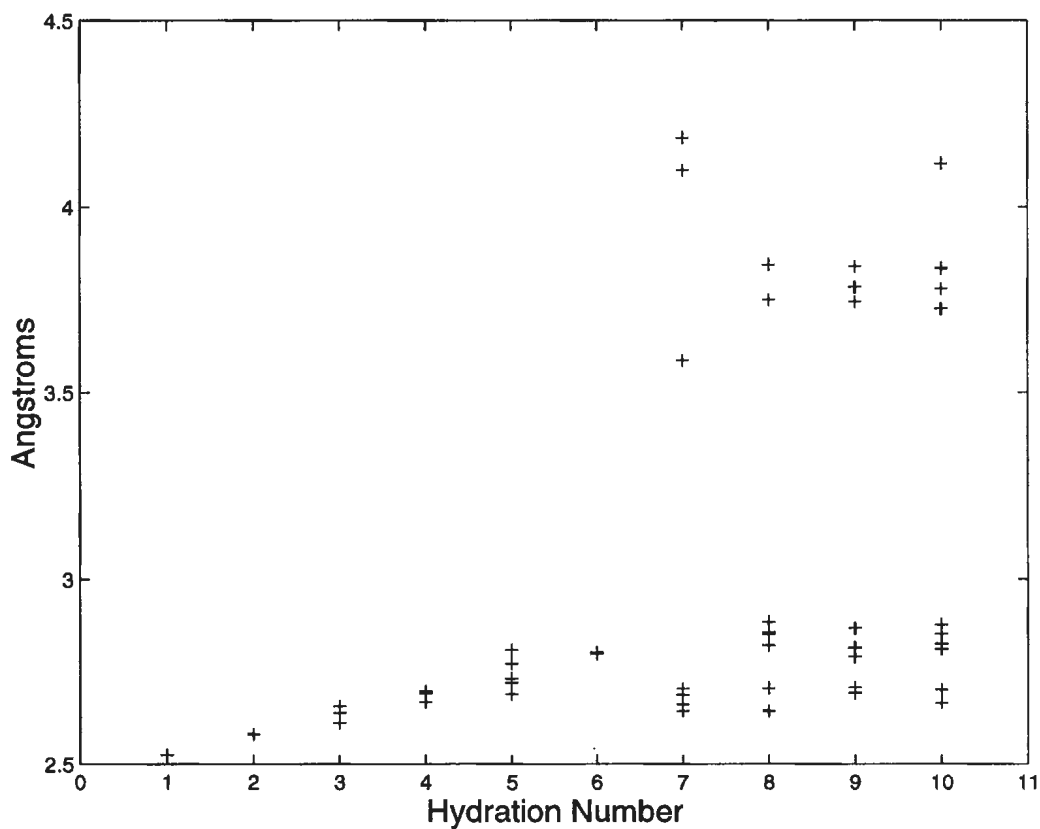


Figure 4.18: Variation of R_{OX} with hydration number for fluoride

to be detected is small. This is supported by the lack of any spectroscopic evidence for multihydrates in aqueous solution. On the other hand, Arshadi and Kebarle (1970) have shown that anions with multiple stages of hydration do exist in the gas phase. In aqueous solution, it may be possible that an anion hydration cage is maintained not by simultaneous hydrogen bonds, but rather a rapid exchange of a single hydrogen bond between the anion and

the other water molecules comprising the cage.

An octahedral coordination model is consistent with *ab initio* calculations as shown in Fig. 4.18. At $n = 6$ the OF distances for each water are essentially equal at 2.80 Å and the complex is octahedral. This value is in excellent agreement with the X-ray diffraction results previously cited. As the number of water molecules in the complex is increased from 1 to 6, the OF distances generally increase, but when additional water molecules are added, a second layer of hydration starts to form about 1 Å beyond the first layer.

An attempt was made to calculate the thermodynamic enthalpy of hydration for the fluoride ion: $F_{(g)}^- \rightarrow F_{(aq)}^-$ $\Delta_s^\infty H = -506 \text{ kJ mol}^{-1}$ (Atkins, 1998). RHF/6-31+G* energies were calculated for F^- , H_2O and fluoride hydrates with up to the $n = 10$ stage of hydration. Association energies were calculated as $E_{F(H_2O)_n} - E_F - nE_{H_2O}$. This energy includes contributions from water-water interactions. These were removed by calculating energies for water clusters and then evaluating $E_{F(H_2O)_n} - E_F - E_{(H_2O)_n}$. The first calculation gave an energy that exceeded the magnitude of $\Delta_s^\infty H$ at $n = 8$ whereas the formation of the same hydrate from a cluster of n interacting water molecules yielded too low a magnitude at least at the $n = 10$ stage,

Table 4.9: Low frequency polarised modes for water clusters calculated at the RHF/6-31+G* level

n	ν (cm ⁻¹)	ρ
2	147	0.22
	187	0.18
3	.	.
4	200	0.01
5	183	0.43
6	168	0.42
	191	0.30
	218	0.44
7	168	0.42
	214	0.49
8	185	0.38

to correct the results to 289K. Considering the simplicity of the model, the agreement between experiment and theory is very good.

Polarised low frequency modes were noted when frequency calculations were performed on the structures used in Fig. 4.19. This may be evidence that the 190 cm⁻¹ isotropic peak of pure water may originate with small water clusters. The vibrational frequency and depolarisation ratio for each structure are listed in Table 4.9.

Chapter 5

Discussion and Conclusion

In this chapter, the experimental and calculated results were compared and critically evaluated. Suggestions for further research were outlined.

5.1 Discussion of Experimental Results

It has been established that the low frequency Raman peaks for aqueous solutions are essentially cation independent (Brooker, 1986). The centre frequency of the band was not changed by more than a few wavenumbers when substantially different cations were used. This small change may be ascribed to the cation influencing the environment of the species causing the low frequency peak. The almost complete independence of the low frequency peak on the cation precludes ion pair interactions as its origin.

In contrast, the effect of changing the anion had a profound effect on

the intensity, frequency and shape of the low frequency band. The band frequency and intensity changed substantially as the anion was changed. The spectra of hydroxide and cyanide showed clear, distinct and unique isotropic low frequency peaks of comparable intensity and band shape with those of the halides. A consistent red shift was observed as the water was substituted first with ^2H and then with ^{18}O . The mass of both the anion and the water molecule had an influence on the band frequency because the force constant in the Born-Oppenheimer approximation was the same for different isotopes. The direction and magnitude of the isotope shift and the general behaviour of the band were entirely consistent with a linear harmonic oscillator for chloride in H_2O and D_2O and qualitatively correct for hydroxide. It was well within the limits of experimental error to propose that the low frequency peaks can be modelled in accordance with the linear harmonic oscillator, Eqn. 2.4 with the anion as one body and a single water molecule as the other. The trend in the intensities along the halides series of hydrates was consistent with the model because their polarisabilities increase with atomic number. Finally, because each band was isotropic, it must have been due to a vibration that was largely symmetric in character. This was the case for the harmonic oscillator model as proposed.

At elevated temperatures, the signals persisted but the centre frequencies shifted down a few wavenumbers. The bandwidth increased and the intensity decreased for the hydroxide and chloride solutions at elevated temperatures. The half width increase was likely due to inhomogeneous broadening where diversity of interactions between the anion hydrate and its environment increased. The anion hydrates existed beyond the normal boiling point of water.

The shapes of the peaks, particularly below half height, suggested the presence of a shoulder on their high frequency side. This may be an overlap from the weak 800 cm^{-1} band of water. This feature was very weak for all but the low frequency band of the iodide spectrum.

On the basis of the experimental data and the theory of Raman spectroscopy, it was concluded that the harmonic oscillator comprising water and an anion as vibrating bodies, in essence a stretching vibration along a hydrogen bond adjoining them, was the origin of the polarised low frequency band.

5.2 Discussion of Theoretical Results

Ab initio calculations have shown conclusively that a species of the type

$A^-\cdot H_2O$ existed for any of the anions on which calculations were performed and that it was stable with respect to the free anion and the water molecule (Table 4.6). There were trends in the geometry amongst the anions but all were monodentate hydrogen bonded structures (Table 4.5).

Animation of the normal mode vibrations of the anion hydrates revealed a unique normal mode for each that appeared to be predominantly a hydrogen stretch between the anion and the water molecule. The only exception was hydroxide for which several modes this motion was present although the second lowest frequency mode was the most dominant in terms of the stretching motion. For cyanide, it was the third lowest. The animated results did show other motions in the normal mode, notably a slight stretch in OH bond adjacent to the hydrogen bond and a small change in orientation the water molecule during the vibration. It was surmised that these motions were energetically insignificant with respect to the hydrogen bond stretch. This was confirmed by the quantitative reproduction of the *ab initio* isotope frequencies by scaling the MP2 frequencies in accordance with Eqn. 2.4. It was concluded that the modes identified are essentially pure hydrogen bond stretches for all but hydroxide.

The agreement between experiment and theoretical frequencies is good,

particularly at the post Hartree-Fock level. The maximum difference between experiment and theory at the MP2 level was for fluoride at about plus 50 percent, and bromide at minus 15 percent. The increase in the difference between the RHF and MP2 results for fluoride is notable and suggests that electron correlation effects are substantial for the fluoride-water interaction. The agreement between the experimental and theoretical MP2 isotope shifts was reasonable for Cl^- in H_2O and D_2O and for $^{18}\text{OH}^-$ in H_2^{18}O but poor for OD^- in D_2O . The experimental shifts were reasonably consistent with Eqn. 2.4 except for OD^- in D_2O .

It is customary to scale *ab initio* results to experimental data to correct for systematic errors (Hehre *et al.*, 1986). When this was done, all MP2 frequencies fell within ten percent of the experimental values except for those of OD^- in D_2O , Br^- in H_2O (both 20 percent too low) and F^- in H_2O which was 40 percent too high. This is notable because scaling has been successfully implemented with few exceptions on a number of molecular systems. The very tight SCF convergence threshold and convergence of several properties to within a few percent on basis sets and levels of theory meant that these differences were not due to inaccuracies in the calculated results.

The difference between the *ab initio* and experimental frequencies for

OD⁻ in D₂O can be explained in terms of anharmonicity. Several normal modes contained a stretching component and the isotope shift calculated using Eqn. 2.4 is much less than the theoretical shift. There is no single normal mode that can be called a pure hydrogen bond stretch and so the harmonic oscillator does not adequately describe the OH⁻·H₂O complex. Experimentally, OH⁻ is known to form other complexes (vanDoren *et al.*, 1987) which may contribute to or otherwise perturb the low frequency band.

The difference between the *ab initio* and experimental frequencies for the fluoride and bromide hydrates did not admit such a simplistic explanation. The theoretical isotope shifts were clearly harmonic and the vibration was accurately described as a stretch along the hydrogen bond for both of these complexes. These results were obtained using Eqn. 2.18 to obtain the normal mode force constants which is strictly valid only for a harmonic potential.

The potential associated with the chloride hydrate stretching mode, Fig. 4.16 is approximately parabolic for only small vibrational amplitudes. These were estimated based on the harmonic RMS amplitude using the expectation value

$$\langle x^2 \rangle = \int_0^{\infty} \psi x^2 \psi dx$$

where ψ is given by Eqn. 2.10 and the Hermite polynomial for the first

excited ($n = 1$) state. Integrating,

$$\langle x^2 \rangle = \frac{3\hbar}{2(\mu k)^{\frac{1}{2}}}$$

from which the RMS amplitude is:

$$x_{\text{RMS}} = \langle x^2 \rangle^{\frac{1}{2}}$$

Using Eqn. 2.4 and the MP2 frequencies to obtain $(\mu k)^{\frac{1}{2}}$, RMS amplitudes of 0.070 and 0.088 Å were obtained for the fluoride and chloride hydrates. These were used as limits over which the cubic regressions were obtained for the potential in Fig. 4.17. against the relative values of R_o and U_o , i.e.,

$$U = \sum_{n=0}^3 c_n x^n$$

This yielded coefficients ($c_0 - c_3$) for the fluoride and chloride hydrate potentials as (0.0, 0.0, 157, -251) and (0.0, 0.0, 46.6 -61.8) respectively. On the basis of the non-zero third order coefficients, it was concluded that the potential surface was not purely quadratic within the RMS amplitude region. More importantly, because of the the very similar ratio of the coefficients, the curves had essentially the same shape and that there was little more anharmonicity in the fluoride surface over that of chloride. The agreement between the experimental and theoretical frequencies was very good for chloride, but poor for fluoride, and the similarity of the relative anharmonicities

suggests the large difference in the latter may originate with a difference in the validity of the isolated molecule approximation for the two systems.

In principle, anharmonicity can be calculated directly from the parameters of the Morse function:

$$V_{(R)} = D_e \left[1 - e^{a(R-R_e)} \right]^2$$

where D_e is the bond dissociation energy. The eigenvalues are:

$$E = \omega_e \left(v + \frac{1}{2} \right) - \overline{\omega_e x_e} \left(v + \frac{1}{2} \right)^2$$

The frequency of the Raman signal is related to the difference in eigenvalues for the $v = 1$ and $v = 0$ states, i.e.,

$$\omega = \omega_e - 2\overline{\omega_e x_e}$$

therefore the effect of anharmonicity is to *decrease* the observed frequency. This would account at least qualitatively for the high value of the calculated frequency for fluoride hydrate if the assumption of harmonicity were erroneous. The Morse potential was not adequate in representing the computed potential at any level of theory, Fig. 4.16 as discrepancies appeared for $R > R_0$. Other empirical potentials were also inadequate in describing the calculated surface.

The decrease in frequency was also predicted by the simple damping model, Eqn. 2.13 but damping should decrease the vibrational frequency of bromide hydrate. The experimental or "damped" value is actually *higher* than the *ab initio* values which do not include the effects of damping.

The large and opposite difference between the calculated and experimental frequencies for bromide and especially fluoride hydrates is compelling motivation for further investigations. For the present, it is postulated that the difference originates with the free molecule approximation and that the normal modes for these anions in condensed phases are influenced by neighbouring molecules. Further work might include an isotopic study of fluoride to determine if the vibration is harmonic in solution. Theoretical work could involve assessing the behaviour of the $A^- \cdot H_2O$ potential surface within a hydration sphere. This could shed light on the extent to which the isolated molecule approximation contributes to this difference.

References

- Abu-Dari, K., K. N. Raymond and D. R. Freyberg, 1979. The Bihydroxide (H_3O_2^-) Anion. A very short Symmetric Hydrogen Bond, *J. Am. Chem. Soc.*, **101**, 13, 3688-3689
- Arshadi, M. and P. Kebarle, 1970. Hydration of OH^- and O_2^- in the Gas Phase. Comparative Solvation of OH^- by Water and the Hydrogen Halides. Effects of Acidity. *J. Phys. Chem.*, **74**, 7, 1483-1485
- Atkins, P., 1998. *Physical Chemistry*, 5th Edition. Oxford University Press, U.K. C16
- Becke, A. D., 1989. Basis-Set-Free Density-Functional Quantum Chemistry. *Int. J. Quantum Chem. Quantum Chemistry Symposium*, **23**, 599
- Beurskens, G. and G. A. Jeffrey, 1964. Crystal Structure of Potassium Fluoride Tetrahydrate. *J. Chem. Phys.*, **41**, 4, 917-923
- Bino, A. and D. Gibson, 1982. The Hydrogen Oxide Bridging Ligand, (H_3O_2^-). 1. Dimerisation and Polymerisation of Hydrolysed Trinuclear Metal Cluster Ions. *J. Am. Chem. Soc.*, **104**, 16, 4385-4388
- Brand, J. C. D. and J. C. Speakman, 1960. *Molecular Structure*. Edward Arnold Publishers, London
- Brooker, M. H., 1986. Raman Spectroscopic Measurements of Ion Hydration, from *The Chemical Physics of Solvation, Part B*. Chapter 4, p 119, Elsevier, Amsterdam
- Brooker, M. H., 1996. Private communication
- Brooker, M. H. and J. D. Craig, 1997. Anion Hydration: Calculated and Measured Raman Frequencies and Intensities. 80th Canadian Society for Chemistry Conference and Exhibition, Windsor, Ontario

- Brooker, M. H. and J. D. Craig, 1999. On the nature of Fluoride Hydration. 82nd Canadian Society for Chemistry Conference and Exhibition, Toronto, Ontario
- Brooker, M. H., O. Faurskov Nielsen and E. Praestgaard, 1988. Assessment of Correction Procedures for Reduction of Raman Spectra, *J. Raman Spectrosc.*, **19**, 71-78
- Combariza, J. E and Kestner, N.R., 1995. Density Functional Study of Short Range Interaction Forces between Ions and Water Molecules. *J. Phys. Chem.*, **99**, 2117-2723
- Decius, J. C., R. M. Hexter, 1977. *Molecular Vibrations in Crystals*, McGraw-Hill Inc., New York
- Engdahl, A and Nelander, B., 1987. On the Relative stabilities of H and D bonded water dimers, *J. Chem. Phys.*, **86**, 4, 1819-1823
- Foresman, J. B., T. A. Keith, K. B. Wiberg, J. Snoonian and M. J. Frisch, 1996. Solvent Effects 5. The Influence of Cavity Shape, Truncation of Electrostatics and Electron Correlation on Ab Initio Reaction Field Calculations. *J. Phys. Chem.*, **100**, 16098
- French, A. P., 1971. *Vibrations and Waves*, W. W. Norton & Company, Inc. New York
- Freund, E., 1973. Étude par spectroscopie Raman-laser des solutions aqueuses de silicates de sodium. Résultats expérimentaux. *Bull. Soc. Chim. France*, N° 7-8, 2238-2224
- Frisch, M. J., Y. Yamaguchi, H. F. Schaefer, III and J. S. Binkley, 1986. Analytic Calculation of Raman Intensities for Closed-Shell Wavefunctions, *J. Chem Phys.* **84**, 531
- Frisch, M. J., G. W. Trucks, H. B. Schlegel, P. M. W. Gill, B. G. Johnson, M. A. Robb, J. R. Cheeseman, T. Keith, G. A. Petersson, J. A. Montgomery, K. Raghavachari, M. A. Al-Laham, V. G. Zakrzewski, J. V. Ortiz, J. B. Foresman, C. Y. Peng, P. Y. Ayala, W. Chen, M. W. Wong, J. L. Andres, E. S. Replogle, R. Gomperts, R. L. Martin, D. J. Fox, J. S. Binkley, D. J. Defrees, J. Baker, J. P. Stewart, M. Head-Gordon, C. Gonzalez and J. A. Pople, 1995. *Gaussian 94, Revision B.3*. Gaussian, Inc., Pittsburgh PA
- Gresh, N., P. Claverie, A. Pullman, 1975. Intermolecular Interactions: Reproductions of the Results of *ab initio* Supermolecule Computations by an

- Additive Procedure. *Int. J. Quantum Chem., Quantum Chemistry Symposium*, **13**, 243-353
- Hehre, W. J., L. Random, P. v.R.Scheleyer, J. A. Pople, 1986. *Ab Initio Molecular Orbital Theory*. J. Wiley & Sons, New York
- Herzberg, G., 1950. *Molecular Spectra and Molecular Structure*, Vol. 1; *Spectra of Diatomic Molecules*. Van Nostrand Reinhold, New York
- Hiraoka, K. and S. Mizuse, 1988. Solvation of Halide Ions with H₂O and CH₃CN in the Gas Phase. *J. Phys. Chem.* **92**, 3943-3952
- Holland, U. and F. Lüty, 1978. Pressure Tuning of the Motional Behaviour of Li⁺, Ag⁺ and Cu⁺ Ions in Shallow Off-centre Potentials of Alkali Halides. *Phys. Rev. B*, **19**, 8, 4298-4314
- Janoschek, R., 1982. Structures, Mobility and IR Spectra of Halide Anion-water Complexes. *J. Mol. Structure*, **84**, 237-343
- Kameda, Y., E. Hidekazu and O. Uemura, 1994. Raman Spectroscopic Study of Concentrated Aqueous LiBr Solutions. *Bull. Chem. Soc. Jpn.*, **67**, 929-935
- Kistenmacher, H., H. Popkie, E. Clementi, 1973. Study of the structure of molecular complexes. III. Energy Surface of a water molecule in the field of a fluorine or chlorine anion, *J. Chem. Phys.*, **58**, 12, 5627-5638
- Kistenmacher, H., H. Popkie, E. Clementi, 1974. Study of the structure of molecular complexes. VIII. Small clusters of water molecules surrounding Li⁺, Na⁺, K⁺, F⁻ and Cl⁻ ions. *J. Chem. Phys.* **61**, 3, 799-815
- Kohn, W. and L. J. Sham, 1965. Self-Consistent Equations Including Exchange and Correlation Effects. *Phys. Rev.* **140**, A1133
- Kollman, P. and Kuntz, I., 1976. Hydration of NH₄F. *J. Amer. Chem. Soc.*, **98**, 22, 6820-6826
- Lee, C. W. Yang and R. G. Parr, 1988. Development of the Colle-Salvetti correlation-energy formula into a functional of the electron density. *Phys. Rev. B* **37**, 785-789
- Luzar, A. and D. Chandler, 1996. Effect of Environment on Hydrogen Bond Dynamics in Liquid Water. *Phys. Rev. Lett.*, **76**, 928-931
- Marechal, E. and Bratos, S., 1978. Infrared and Raman spectra of hydrogen bonded liquids. Effect of electrical anharmonicity on profiles of hydrogen-stretching bands. *J. Chem. Phys.*, **68**, 4, 1825-1828

- McQuarrie, D. A., 1976. *Statistical Mechanics*. Harper & Row Publishers Inc.
- McQuarrie, D. A., 1983. *Quantum Chemistry*. University Science Books
- Mizoguchi, K., Y. Hori and Y Tominaga, 1992. Study on the dynamical structure in water and heavy water by low-frequency Raman Spectroscopy. *J. Chem. Phys.* **97**, 3, 1961-1968
- Morse, P. M., 1929. Diatomic Molecules According to the Wave Mechanics. II. Vibrational Levels. *Phys. Rev.* **34**, 57
- Murphy, W. F., M. H. Brooker, O. Faurskov Nielsen, E. Praestgaard and J. E. Bertie, 1989. Further assessment of reduction procedures for Raman spectra *J. Raman Spectroscopy*, **20**, 695-699
- Nielsen, O. F., 1993. Low Frequency Spectroscopic Studies of Interactions in Liquids. *Annu. Rep. Prog. Chem., Sect. C, Phys. Chem.*, **90**, 3-44
- Payzant, J. D., R. Yamdagni, P. Kebarle, 1971. Hydration of CN^- , NO_2^- , NO_3^- and OH^- in the Gas Phase. *Can. J. Chem.*, **49**, 3308-3313
- Poirier, R. A., Peterson, M. R. and Yadav, A., 1995. *MUNGAUSS*. Department of Chemistry, Memorial University of Newfoundland, Canada
- Pople, J. A., P. M. W. Gill and B. G. Johnson, 1992. Kohn-Sham density-functional theory within a finite basis set. *Chem. Phys. Lett.*, **199**, 557
- Pople, J. A., H. B. Krishnan, H. B. Schlegel, J. S. Binkley, 1979. Derivative Studies in Hartree-Fock and Møller-Plesset Theories. *Int. J. Quantum Chem., Quantum Chemistry Symposium*, **13**, 225
- Pople, J. A., Schlegel, H. B., Krishnan, R., Defrees, D. J., Binkley, J. S., Frisch, M. J., Whiteside, R. A., Hout, R.F., Hehre, W. J., 1981. Molecular Orbital Studies of Vibrational Frequencies. *Int. J. Quantum Chem., Quantum Chemistry Symposium*, **15**, 269
- Pye, C.C., R. A. Poirier, D. Yu, P. R. Surján, 1994. *Ab Initio* Hartree-Fock calculations of the interaction energy of bimolecular complexes. *J. Mol. Structure*, **307**, 239-259
- Ratajczak, H. and W. J. Orville-Thomas, 1980. *Molecular Interactions*. Vol. I. John Wiley & Sons Ltd.
- Rice, B. C., 1984. M.Sc. Thesis. Memorial University of Newfoundland, St. John's Newfoundland, Canada

- Schrötter, H. W. and H. W. Klöckner, 1979. *Topics in Current Physics, Vol. 11: Raman Spectroscopy of Gases and Liquids*, A. Weber, editor. Springer-Verlag Berlin Heidelberg.
- Sharpe, A. G., 1990. The Solvation of Halide Ions and its Chemical Significance. *J. Chem. Ed.* **67**, 309
- Simons, J. and Nichols, J., 1997. *Quantum Mechanics in Chemistry*. Oxford University Press
- Svendsen, E. N., 1979. Calculation of Raman Intensities. *Int. J. Quantum Chem., Quantum Chemistry Symposium*, **13**, 553
- Szabo A. and N. S. Ostlund, 1996. *Modern Quantum Chemistry*. Dover Publications Inc., New York
- Szász, G. I. and K. Heinzinger, 1983. A Molecular Dynamics Study of an Aqueous CsF Solution. *Z. Naturforsch.* **38a**, 214-224
- Terpstra, P., D. Combes and A. Zwick, 1990. Effects on dynamics of water: A Raman spectroscopy study. *J. Chem. Phys.*, **92**, 1, 65-70
- Tödheide, K., 1972. in F. Franks, (Ed.) *Water: a Comprehensive Treatise*, Vol. 1. Plenum, New York.
- vanDoren, J. M., S. E. Barlow, C. H. Depuy and V. M. Bierbaum, 1987. Collisional dissociation of small hydroxide ion-water clusters. *Int. J. Mass. Spectrom. Ion Proc.*, **81**, 85-92
- Walrafen, G. E., Y. C. Chu, 1992. Low Frequency Raman Spectra from Concentrated Aqueous Hydrochloric Acid. Normal Coordinate Analysis Using a Four Atomic Model of C_s Symmetry. *J. Phys. Chem.*, **96**, 23, 9127-9132
- Wilson, E. B., J. C. Decius, P. C. Cross, 1955. *Molecular Vibrations: The Theory of Infrared and Raman Vibrational Spectra*. McGraw-Hill Book Company
- Wong, M. W., M. J. Frisch and K. B. Wiberg, 1991. Solvent Effects 1. The Mediation of Electrostatic Effects by Solvents. *J. Am. Chem. Soc.*, **113**, 4776
- Wong, M. W., K. B. Wiberg and M. J. Frisch, 1992. Solvent Effects 2. Medium Effect on the Structure, Energy, Charge Density, and Vibrational Frequencies of Sulphamic Acid. *J. Amer. Chem. Soc.*, **114**, 523
- Wong, M. W., K. B. Wiberg and M. J. Frisch, 1991. SCF Second Derivatives and Electric Field Properties in a Reaction Field. *J. Chem. Phys.*, **95**, 8991

- Xantheas, S. S., Dunning, T. H, 1996. Structures and Energetics of $F^-(H_2O)_n$, $n= 1-3$, Clusters from *ab Initio* Calculations. *J. Phys. Chem.*, **98**, 51, 13489-13497
- Xantheas, S. S., Dang, L. X., 1996. Critical Study of Fluoride-Water Interactions. *J. Phys. Chem.*, **100**, 10, 3989-3995
- Xuefeng, Z., Fogarasi, G, Lium R and Pulay, 1993. Building a database of force constants based on scaled *ab initio* (SQM) results. I. Chlorobenzenes. *P. Spectrochimica Acta*, **49A**, 10, 1499
- Yamaguchi, Y., Frisch, M., J. Gaw, H. F. Schaefer III and J. S. Binkley, 1986. Analytic Evaluation and Basis Set Dependence of Intensities of Infrared Spectra. *J. Chem. Phys.* **84**, 4, 2262

Appendix A

Data Acquisition Code

```
rem reads serial asynchronous output (rs232) of dec writer/black-box
rem data acquisition system for Coderg Raman spectrometer. J. Craig
rem 19 Oct 1995/ 31 Jan 1996/ 23 Oct 1997/ 19 Oct 1998
rem RA4.BAS
cls : print : print "Data acquisition program. Data will be written to the"
print "    specified file. Enter 'Q' to stop acquisition. "
5 for i=1 to 54 : print chr$(236); : next i : print
input "File name";f$ : f$=ucase$(f$)
print f$;" opened. Ready for data."
open "com1:300,e,7,1,cs,ds" as #1
open f$ for output as #2
byte=-1                      rem data byte count
b$=""
while b$<>"Q"
  while instat<>-1
    while loc(1)<>0
      a$=input$(1,#1)
      byte=byte+1
      if byte>0 then          rem eliminate 1st blank line
        print a$;
        print #2, a$;
        if asc(a$)=13 then
          print #2, chr$(10); rem insert a line feed after <cr>
        end if
      end if
    wend
  wend
  b$=ucase$(inkey$)
wend
close (1) : close (2)
print : print "Data acquisition terminated by user."
print byte;" bytes written to ";f$ : print
input "Do another run";x$
if ucage$(left$(x$,1))<>"N" then
  goto 5
end if
32767 end
```

Appendix B

Reduced Spectrum and Baseline Calculations

```
c Data treatment: polarised and depolarised spectra are independently
c averaged, and smoothed. This program reads header information and
c and intensity data generated by the smoother program SMOOTHN and writes
c a file containing npoints,Y data in a format that is compatible with
c GRAMS, PLOTTEK.PAS or (x,y) format (wavenumber and R intensity).
c The program is first run on the polarised smoothed spectra and the
c autoscale option is selected. When it is run on the depolarised spectrum
c the scaling factor calculated from the polarised data is used.
```

```
c Variables: n points per wave number, nu_s starting wave number
c nu(i) wavenumber, nu_e exciting wavenumber, inten intensity, hinfo,hcon
c header information and constants.
```

```
c Transcribed from the original BASIC version of A. N. Betz (1976)
c by J. Craig. Character functions written by A. Goulding
```

```
c Original documentation follows:
```

```
c REM This program takes a real array input and baseline corrects
c REM by subtracting the lowest value from all points. Option is
c REM available for R2(v), R(v), or second moment function as well.
c revised by jcraig 18 Jul 1997; revised formats for data output and
c scale factor 7 Mar 1998
```

```
program      basr
implicit    none
intrinsic   max,min
integer     i
real        y, hcon(6),inten(8000),nu(8000),k
real        ty,nu_s,nu_e,n,t,npoints,spbc,s
real        maxr,minin
character*80 hinfo,infil,outfil
character*7  fil
character*1  q,fmt,ftn
character    upcase
character*15 stripblank
```

```

1008 format (a79)
2002 format (1x,f8.4)
2004 format (1x,f7.1,1x,f8.3)
5001 format (a)
6001 format (1x,a78)
6002 format (' Please enter file name.....: ', $)
6004 format (' Select output (T)ekplot, (G)rams, or [X],Y....: ', $)
6006 format (' Output will be written to.....: ', a22)
6011 format (' Input starting point for baseline, usually 2.: ', $)
6013 format (' Select function: [R] [I(v)*(1-exp(-hv/kT))],')
6014 format (' (N)one, (S)econd moment[I(v)*v^2] or')
6015 format (' (2) [I(v)*v*tanh(hv/2kT)].....: ', $)
6016 format (' Enter scale factor or (1) none or (0) auto....: ', $)
6018 format (' Scale factor used .....: ', f8.6)
6020 format (' CURRENT FILE DESCRIPTION IS: ', /a)
6022 format (' Do you wish to change description? (Y/N).....: ', $)
6024 format (' Enter new description (max 80 characters)....: ')
6029 format (' Conversion complete.')
```

```

write (6,6002)
read (5,5001) fil
infil = fil
write (6,6004)
read (5,5001) fmt
fmt = upcase(fmt)
if (fmt.eq.'G') then
  outfil = fil//'.prn'
else if (fmt.eq.'T') then
  outfil = fil//'.r'
else
  outfil = fil//'.dat'
end if
outfil = stripblank(outfil)
write (6,6006) outfil
write (6,6011)
read (5,*) spbc
write (6,6013)
write (6,6014)
write (6,6015)
read (5,5001) ftn
write (6,6016)
read (5,*) S

open (1,file=infil,status='old')
open (2,file=outfil,status='unknown')
read (1,1008) hinfo
if (fmt.eq.'T') then
  write (6,6020) hinfo
  write (6,6022)
  read (5,5001) q
  if (upcase(q).eq.'Y') then
    write (6,6024)
    read (5,5001) hinfo
  end if
  write (2,1008) hinfo
end if
do i=1,6
```

```

        read (1,*) hcon(i)
        if (fmt.eq.'T') then
            write (2,*) hcon(i)
        end if
    end do

    i = 0
    n = hcon(4)
    t = hcon(5)
    ty = hcon(1)
    nu_e = 1.0/hcon(2)*1e8
    nu_s = hcon(3)
    maxr = 0.0
    minin = 1000.0
    npoints = hcon(6)

0001 read (1,*,end=2) y
        i = i+1
        if (i.gt.spbc) then
            minin = min(y,minin)
        end if
        nu(i) = nu_s+(i-1)/n
        inten(i) = y
        goto 1
0002 close (1)

    if (i.ne.npoints) then
        write (6,*) 'Erroneous data count'
        stop
    end if
    close (1)

    do i=1, npoints
        inten(i) = inten(i)-minin
        IF (inten(i).lt.0) then
            inten(i) = 0
        end if
        inten(i) = inten(i)*(nu_e/(nu_e-nu(i)))**4
    end do

    q = upcase(ftn)
    if (q.ne.'N'.and.q.ne.'S'.and.q.ne.'2') then
        do i=1,npoints
            k = nu(i)*1.43879/T
            inten(i) = inten(i)*nu(i)*(1-exp(-k))
        end do
    end if
    if (q.eq.'S') then
        do i=1,npoints
            inten(i) = inten(i)*nu(i)**2
        end do
    end if
    if (q.eq.'2') then
        do i=1,npoints
            k = nu(i)*1.43879/(2*T)
            inten(i) = inten(i)*nu(i)*((exp(k)-exp(-k))/(exp(k)+exp(-k)))
        end do
    end if

```

```

        end if

if (S.eq.0) then
    maxr = 0.0
    do i=1, npoints
        maxr = max(inten(i),maxr)
    end do
    S = 999.0/maxr
end if
write (6,6018) s
fmt = upcase(fmt)

do i=1, npoints
    inten(i) = inten(i)*S
    if (fmt.ne.'T') then
        write (2,2004) nu(i),inten(i)
    else
        write (2,2002) inten(i)
    end if
end do
close (2)
write (6,6029)
END

function upcase(c)

intrinsic char,ichar
character*1 c,upcase

if (c.ge.'a'.and.c.le.'z') then
    upcase = char(ichar(c)+ichar('A')-ichar('a'))
else
    upcase = c
end if
return
end

character*(*) function stripblank(string)

character*(*) string
integer i,j

do i = 1,LEN(string)
    j = i+1
    do while ((string(i:i) .eq. ' ') .and. (j .le. LEN(string)))
        string(i:i) = string(j:j)
        string(j:j) = ' '
        j = j + 1
    end do
end do
stripblank = string
return
end

```

Appendix C

Example XY Plot File

```
% rplot2.m Matlab file to plot Raman spectra and
% generate an isotropic file. 24 Jan 1998
% jcraig 10 March 1998, 26 June 1998, 6 Oct 1998

clear all
clf
pfile=input('Enter polarised file name.... ', 's');
dfile=input('Enter depolarised file name.. ', 's');
pp =input('Plot parallel and perpend.... ', 's');
l =length(pfile);
ifile=pfile(1:l-1);
ifile=[ifile 'i'];
fp =fopen(pfile,'r'); % open polarised and
fd =fopen(dfile,'r'); % depolarised files for reading
fi =fopen(ifile,'w'); % write to isotropic file
P =fscanf(fp,'%g %g',[2 inf]);
D =fscanf(fd,'%g %g',[2 inf]);
n =min(length(P),length(D)); % number of pts in shorter file
nu =P(1,(1:n)); % vector of wave numbers
ip =P(2,(1:n)); % vector of intensities
id =D(2,(1:n));
ii =ip-(4/3).*id; % compute isotropic intensity
fprintf(fi,' %6.2f %7.2f\n',[nu;ii]);
fclose(fp);
fclose(fd);
fclose(fi);
if ~isempty(pp)
    H=plot(nu,ip); %ip+200);;
    oaxis=axis;
    axis([0 max(nu)+50 -50 oaxis(:,4)])
    hold on
    I=plot(nu,id); %id+100);
    end
J=plot(nu,ii);
xlabel('Frequency (cm-1)','fontsize',15)
ylabel('R (relative)','fontsize',15)
```

Appendix D

Example *ab initio* Input File

A file with this format is used to instruct the *ab initio* computational package to perform the required calculations. It includes a specification of the basis set, level of theory and provides an initial starting geometry. A frequency calculation is requested.

```
%chk=uuh2ofmp
#P mp2/6-311++G** opt SCF=DIRECT

<<><H2OF-

-1 1
F
O      F      OF
H1     0      OH1   F   FOH
H2     0      OH2   H1  HOH   F   T1

OF          2.4379
OH1         1.0521
OH2         0.9581
FOH         2.8099
HOH        100.6394
T1          -0.

--Link1--
%chk=uuh2ofmp
#P mp2/6-311++G** FREQ GEOM=CHECKPOINT GUESS=READ SCF=DIRECT

fh2o- freq

-1 1
```





